RESEARCH ARTICLE

Exercise and Cardiac Remodeling in Normal and Athletic States

An integrated mathematical model of the cardiovascular and respiratory response to exercise: model-building and comparison with reported models

Carlos Andrés Sarmiento,[1] Alher Mauricio Hernández,[1] Leidy Yanet Serna,[2,3] and Miguel Ángel Mañanas[2,3]

[1]*Bioinstrumentation and Clinical Research Group, Bioengineering Program, Universidad de Antioquia UdeA, Medellin, Colombia;* [2]*Department of Automatic Control and the Biomedical Engineering Research Centre of The Universitat Politècnica de Catalunya, Barcelona, Spain; and* [3]*Biomedical Research Networking Center in Bioengineering, Biomaterials, and Nanomedicine (CIBER-BBN), Madrid, Spain*

Abstract

The use of physiological models in medicine allows the evaluation of new hypotheses, development of diagnosis and clinical treatment applications, and development of training and medical education tools, as well as medical device design. Although several mathematical models of physiological systems have been presented in the literature, few of them are able to predict the human cardiorespiratory response under physical exercise stimulus adequately. This paper aims to present the building and comparison of an integrated cardiorespiratory model focused on the prediction of the healthy human response under rest and aerobic exercise. The model comprises cardiovascular circulation, respiratory mechanics, and gas exchange system, as well as cardiovascular and respiratory controllers. Every system is based on previously reported physiological models and incorporates reported mechanisms related to the aerobic exercise dynamics. Experimental data of 30 healthy male volunteers undergoing a cardiopulmonary exercise test and simulated data from two of the most current and complete cardiorespiratory models were used to evaluate the performance of the presented model. Experimental design, processing, and exploratory analysis are described in detail. The simulation results were compared against the experimental data in steady state and in transient regime. The predictions of the proposed model closely mimic the experimental data, showing in overall the lowest prediction error (10.35%), the lowest settling times for cardiovascular and respiratory variables, and in general the fastest and similar responses in transient regime. These results suggest that the proposed model is suitable to predict the cardiorespiratory response of healthy adult humans under rest and aerobic exercise conditions.

NEW & NOTEWORTHY This paper presents a new cardiorespiratory model focused on the prediction of the healthy human response under rest and aerobic dynamic exercise conditions. Simulation results of cardiorespiratory variables are compared against experimental data and two of the most current and complete cardiorespiratory models.

aerobic exercise; cardiorespiratory system; computer simulation; mathematical model; regulatory mechanisms

INTRODUCTION

The cardiorespiratory system comprises the union of elements, relations, functions, and interactions of cardiovascular and respiratory systems and their respective regulatory mechanisms. Both systems show a variety of mechanisms with complex and different dynamics oriented to maintain the physiological homeostasis despite different pathologies and external disturbances (1, 2). The variables resulting from the complex regulation processes of both systems have an important role in clinical applications of diagnosis, monitoring, and treatment because they allow for evidencing the correct physiological functioning (3).

Physical exercise is a natural stimulus related to the increase in metabolic activity that is able to generate significant organism variations that cannot be displayed under resting conditions (4). These changes are especially related to the respiratory and cardiovascular systems due to their important role in the regulation of the high levels of cardiac output and oxygen supply required by the tissues (5, 6). For this reason, and as a result of the well-defined pattern shown in healthy human subjects, the cardiorespiratory response analysis under dynamic exercise is recognized as a valuable tool for the diagnosis, monitoring, and prevention of diseases, medical treatment evaluation, postoperative recovery evolution, and sports analysis (4, 6–8).

Computational modeling and simulation have been proposed as a tool to improve the understanding of the complex interactions and functions of physiological systems and to predict their response under different stimuli (9, 10). Its use in the clinical area allows the execution of virtual experiments, evaluation of new hypotheses, development of diagnosis and clinical treatment applications, development of training and medical education tools, and medical equipment design (10, 11).

Several cardiovascular, respiratory, and cardiorespiratory models have been presented in the literature, but few of them are able to adequately simulate the physical exercise stimulus. The development considerations, the specificity of its application, and the strictness of the physiological systems' description involve characteristics and restrictions that can constrain the model simulation under a specific stimulus. For instance, the models by Lu et al. (12) and Ellwein et al. (13) are detailed in their description of several cardiovascular and respiratory dynamics, but they neglect aspects of neural control and do not include the prediction of critical cardiorespiratory variables associated with exercising. The models proposed by Poon et al. (14), by Fincham and Tehrani (15), and by Magosso and Ursino (16) involve some sophisticated regulatory mechanisms, among them one related to physical exercise. However, they are specialized only in the cardiovascular or respiratory system constraining their applications for a complete cardiorespiratory analysis. Similarly, the model by Cheng et al. (17) is one of the most complete and evaluated cardiorespiratory models, but it is not suitable for the physical exercise simulation due to its development specificity, which is mainly focused on the sleep mechanism (18, 19). Other current works, such the cardiorespiratory models by Albanese et al. (20) and Serna et al. (21), have tried to overcome previous models' restrictions by including more precise cardiorespiratory interactions or better neuronal control dynamics for the exercise stimulus, but there are no studies that evaluate which of them are more suitable for the physical exercise simulation.

The aim of this work is to present the building of an integrated cardiorespiratory model focused on the prediction of the healthy human response under rest and aerobic dynamic exercise conditions and compare it under a structural approach against experimental data and versus two of the most current and complete cardiorespiratory models. The model includes the cardiovascular system, the respiratory mechanics and gas exchange system, and the cardiovascular and respiratory controllers, each one based on previously validated cardiovascular and respiratory models to represent the response under resting conditions (21–24). To focus the model on the prediction of physiological behavior under aerobic exercise, validated models of several mechanisms related to the stimulus were incorporated and adapted. The mechanisms include the ventilatory demand estimation as a function of metabolic activity, a respiratory control approach focused on the mechanical work minimization, the influence of the central motor command and central respiratory neuromuscular drive on the autonomic nervous cardiac activity, the specific cardiovascular description and local metabolic vasodilation mechanisms of the active muscles, and the effects of respiration and muscular contractions on venous return. This model would be useful for clinical researches

and applications, mainly those related to the analysis and evaluation of the response of healthy human subjects under different conditions and exercise levels. Furthermore, after a specific fitting and validation, the model can also be used for applications related to the analysis of cardiorespiratory diseases, simulation of therapeutic interventions, and personalized diagnostic tools.

The present paper provides a model description and shows the results of a structural comparison against other cardiorespiratory models under simulation of aerobic exercise. The models selected for the comparison are two of the most current and complete cardiorespiratory models available in the literature: the model proposed by Albanese et al. (20) and the model proposed by Serna et al. (21). Experimental data from healthy human volunteers during a cardiopulmonary exercise test were used as a reference for the evaluation of results. First, the experimental design related to the cardiopulmonary exercise test and the processing applied to the experimental data are described. Then, the description of the mathematical model and the values of the assigned parameters are explained in qualitative terms, detailing the characteristics of each subsystem and emphasizing the aspects of the exercise mechanisms. An exploratory analysis of the experimental data, aimed to evaluate the dynamics of the cardiorespiratory variables, is performed. The comparison strategy between models regarding the experimental data is described, which includes the standardization of the simulation conditions, the evaluation methods, the computational implementation, and the data analysis. Then, the simulation results under exercise stimulus of the proposed model, the model by Serna et al. (21), and the model by Albanese et al. (20) are compared with the experimental data in steady state and in transient regime. Finally, a sensitivity analysis focused on evaluating the individual role of each exercise mechanism included and adapted to the built model is presented.

METHODS

In this work, all the symbols related to the model parameters are in italics in order to clearly differentiate them from model variables. Time-varying signals are considered as variables, i.e., that change with time during the model simulation. The parameters, as defined by the models of the systems, controllers, and mechanisms included, are assumed as constant values or inputs of the model that do not change with time, although they could vary in a more detailed future approach.

Experimental Design

Subjects.

All procedures and protocols conformed to the Declaration of Helsinki and were approved by the Human Research Ethical Committee of the Department of University Research (SIU) of the University of Antioquia (approval certificate 17-59-711). The information about the protocols and possible risks related to the experiment was reported to all subjects before they gave their written consent to participate.

Thirty healthy male volunteers participated in the study [28.3 ± 6.9 yr old, 173.6 ± 6.0 cm height, 76.5 ± 9.3 kg weight, 25.4 ± 2.8 body mass index (BMI), and Hispanic ethnicity]. All subjects were nonsmokers, with an age range between 18

and 48 yr and with BMI <30 kg/m^2, none had pacemakers or any other kind of electrical stimulator implanted, and none had a history or symptoms of cardiovascular, pulmonary, metabolic, or neurological disease. The physical fitness in our group was not homogeneous and ranged from sedentary subjects to subjects under physical training (<15 h/wk).

The Kruskal-Wallis rank test was used to calculate the experimental sample size (25), assuming a probability function with distribution free, a 95% statistical power, a P value of 0.05, and signal measurement variability <15%.

Exercise test.

All subjects performed a cardiopulmonary exercise test (CPET) 2 h after a light breakfast (9 AM). Strenuous physical activity, alcohol, caffeinated beverage, and psychoactive substances consumption were prohibited 24 h before the testing session. All tests were conducted with close medical supervision in a laboratory under controlled environmental conditions (ambient temperature of 26.6 ± 1.7°C, relative humidity of 64.0 ± 5.1%, and an atmospheric pressure of 640 mmHg).

A programmable load cycle ergometer model LC6 Monark was used in this experiment. The cycle ergometer was calibrated before each test to guarantee the same conditions. The seat and handlebar positions were adjusted for every subject according to the manufacturer's recommendations, with the same body posture always kept in every test.

The participants performed an incremental, submaximal, and multistate exercise test at a constant pedaling rate of 60 rpm, based on the protocol proposed by Latin et al. (26). The test duration was 45 min, divided into five phases controlled and monitored by software (see *Equipment and measurements*). Table 1 summarizes the phases of the test. The indications for the terminating test were heart rate measurements bigger than the 85% of the maximum heart rate [HR; the highest value of HR that can be attained and measured during incremental exercise, usually predicted as 220-age (7, 27)], inability to maintain the imposed pedaling rate, the subject's desire to stop, and the recommendation of the medical staff or at the end of the test.

After anthropometric measurements, a forced spirometry test, familiarization with the test procedures, and the necessary instrumentation were done, subjects were asked to remain at rest, sitting on the cycle ergometer for 2 min while baseline measurements were made. The exercise began with 4 min of warmup at 0 W of load, followed by an incremental exercise phase of five constant load steps, with load increases of 25 W and a duration of 5 min each. The recovery phase consisted of four constant load states, with successive load reduction of 25 W and a duration of 1 min each, followed by 5 min of 0 W. Finally, subjects were asked to remain at

rest for 5 min to ensure that the vital signs reached their resting behavior. The pedaling rate was kept constant during *phases 2, 3,* and *4* and was shown during the test to the subject through the cycle ergometer screen.

The selection of the cycle ergometer is justified by a lower presence of motion artifacts in signals, the reduced presence of ambient noise in the measurements, and the correct measurement of noninvasive blood pressure (7), besides having been implemented in experiments used to validate mathematical models referenced in this work (16). A submaximal exercise test was chosen considering the lower risk for sedentary or not necessarily trained subjects (7). The time distribution of the incremental exercise phase was selected to reach steady-state variable measurements (8, 26, 28). The pedaling rate was selected considering that, compared with other usually implemented values, the highest oxygen consumption values are produced at 60 rpm (8). Finally, the number of phases, their function, and loads were determined according to recommendations and results of similar previous works (8, 28, 29).

Another important aspect is related to the subject's posture during the test. The models implemented in this work specify their application for supine posture because they do not integrate mechanisms that consider the body pressure changes, and the experimental data used for their validation correspond to this condition. Even so, in this work, the experimental measurements in sitting posture will be taken as a reference considering that it is an usual condition in cardiopulmonary exercise tests, and a different but constant posture generates a constant difference in physiological variables (30).

Equipment and measurements.

Cardiovascular and respiratory variables, including gas exchange variables, usually analyzed in cardiopulmonary exercise tests, were recorded. The oxygen uptake ($\dot{V}O_2$), carbon dioxide production ($\dot{V}CO_2$), end-tidal oxygen partial pressure (PETO$_2$), end-tidal carbon dioxide partial pressure (PETCO$_2$), total minute ventilation ($\dot{V}E$), inspiratory time (TI), tidal volume (VT), breathing frequency (BF), and HR were collected using the automatic respiratory gas analysis system Oxycon mobile. Measurements of systolic blood pressure (PS), diastolic blood pressure (PD), and mean arterial blood pressure (PM) were recorded using the General Electric Procare B20 vital signs monitor. The ventilatory and gas exchange variables were monitored continuously during all of the test with a sampling frequency of 2.0 Hz, making the subjects breathe through a face mask connected to the respiratory gas analysis system; the HR was calculated automatically and continuously monitored during all of the test from a three-lead electrocardiogram embedded in the respiratory gas analysis system and collected with a sampling frequency of 2.0 Hz, and PS, PD, and PM were measured twice at different times, 1 min before the end of each phase and 4 min after a load increase during the incremental exercise phase, using a sized blood pressure cuff placed on the left arm according to the standard recommendations. The automatic respiratory gas analysis system was calibrated before each test according to the specifications of the manufacturer.

Table 1. *Test phases*

Phase	Description	Duration, min
1	Rest	2
2	Warming	4
3	Incremental exercise	25
4	Recovery	9
5	Rest	5

All records and measurements were made by the software of each equipment. The setup and control of the exercise test were performed by the gas analysis system software.

Experimental Data Processing

Data conditioning and exploratory analysis.
Although the recorded variables were previously filtered by the measurement equipment, basic data conditioning was applied to reduce the influence of noise and artifacts sources. A moving average low-pass filter with a 3-s window, in both forward and reverse directions, was applied for continuous measurements. The average of the last minute of each continuous measurement for each subject was used as a representative sample of each phase of the exercise test at steady-state conditions.

In order to analyze the experimental physiological response under exercise, the sensitivity and linearity of each recorded cardiorespiratory variable as a function of the load were evaluated. The first measure represents the sensitivity of the variable with respect to the stimulus increase, whereas the second one allows us to evaluate the behavior as quantification of similarity regarding a linear tendency. The sensitivity and linearity for each physiological variable were represented as the slope and coefficient of determination, respectively, both applied only to the representative data from the warming and incremental exercise phases. All data were normalized by the corresponding warming value to compare the slopes of different variables. In this sense, slopes with the largest magnitudes correspond to highly sensitive variables, whereas coefficients of determination close to 100% are related to highly linear variables.

Estimation of partial pressures of alveolar gasses.
In order to compare the experimental data with the simulation results of the models regarding the gas exchange system, and considering that the available measurements of $PETO_2$ and $PETCO_2$ are not directly predicted by cardiorespiratory models, estimations of alveolar oxygen partial pressure (PAO_2) and alveolar carbon dioxide partial pressure ($PACO_2$) were calculated. Although arterial oxygen partial pressure (PaO_2) and the arterial carbon dioxide partial pressure ($PaCO_2$) are more directly related to the cardiorespiratory regulation processes, its relationship with $PETO_2$ and $PETCO_2$ involves more complex dynamics, and its estimation demands approximations that may constraint its application. The equations reported in the work of Van Iterson et al. (31) and Wasserman et al. (6) for $PACO_2$ and PAO_2, respectively, correspond to the following expressions.

$$PACO_2 = 5.5 + 0.9PETCO_2 - 0.0021VT \qquad (1)$$

Equation 1 allows for estimating $PACO_2$ in mmHg from the value of $PETCO_2$ in mmHg and VT in ml. This expression is the result of a study focused on the evaluation of the difference between $PETO_2$ and $PACO_2$ under an exercise test (32) and has been applied in different works (33).

$$PAO_2 = FiO_2 (P_{atm} - 47) - PACO_2 \cdot \frac{\dot{V}O_2}{\dot{V}CO_2}. \qquad (2)$$

According to *Eq. 2*, PAO_2 in mmHg can be estimated from the values of the inspired fraction of dry oxygen (FiO_2), the atmospheric pressure (P_{atm}) in mmHg, the ideal $PACO_2$ in

mmHg, and the ratio between $\dot{V}O_2$ and $\dot{V}CO_2$. Other expressions were evaluated for the PAO_2 estimation, but they correspond to indirect use of the same equation or simplifications (7, 21, 34, 35).

It is highlighted that both equations provide approximations to physiological variables that are difficult to measure experimentally, that have been implemented in different works related to exercise (7, 28, 31, 33, 34), and were selected as a result of a comprehensive review and comparison regarding the expected for the experimental conditions.

Data restriction to aerobic exercise.
Considering that the cardiorespiratory models do not include mechanisms to simulate the anaerobic metabolic activity, the experimental data to be compared with the model's simulation results were limited to the anaerobic threshold (*AT*) of each subject. *AT* was calculated using the noninvasive technique v-slope that identifies the $\dot{V}O_2$ value for which the change in the linear slope of the relationship of $\dot{V}CO_2$ to $\dot{V}O_2$ occurs (28). The implemented algorithm has been described by Hernández (18). Although it is not required for the subsequent processing of the data, the ventilatory threshold values are also presented due to their importance as reference values of the cardiopulmonary tests and for the calculation of *AT*.

Model Building

The present model (CR1) is a self-regulated cardiorespiratory model that comprises cardiovascular circulation, respiratory mechanics, and gas exchange system as well as cardiovascular and respiratory controllers. Every system and controller are based on previous physiological models and incorporate reported models of several mechanisms related to the aerobic exercise dynamics. The schematic block diagram of CR1 is shown in Fig. 1, and the symbols are described in Table 2. The adapted or modified mechanisms include *1*) the estimation of ventilatory demand as a function of brain carbon dioxide partial pressure ($PbCO_2$), PaO_2, $PaCO_2$, and metabolically related neural drive component to the ventilation (MRV), *2*) a respiratory control approach focused on mechanical work of breathing minimization, *3*) the action of the central command on cardiovascular efferent sympathetic and parasympathetic control activities, *4*) the influence of the central respiratory neuromuscular drive on cardiovascular efferent sympathetic and parasympathetic control activities, *5*) a separate description of vascular beds in active and resting skeletal muscles, *6*) the local vasodilation of the active muscles, *7*) the effect of muscular contractions on venous return (muscle pump), *8*) the effect of respiration on venous return (respiratory pump), and *9*) use of the blood flow signals from the cardiovascular system in the gas exchange and mixing compartment.

Cardiovascular system.
The model of the cardiovascular system is based on the work by Ursino and Magosso (24). It includes the pulsating heart, pulmonary circulation, and systemic circulation. The heart model comprises both the right and left heart, with each composed of a passive atrium and a pulsatile ventricle. It considers the blood flow through the mitral, aortic, tricuspid, and pulmonary valves. Pulmonary circulation includes vascular beds such as pulmonary arteries, peripheral vessels, and pulmonary
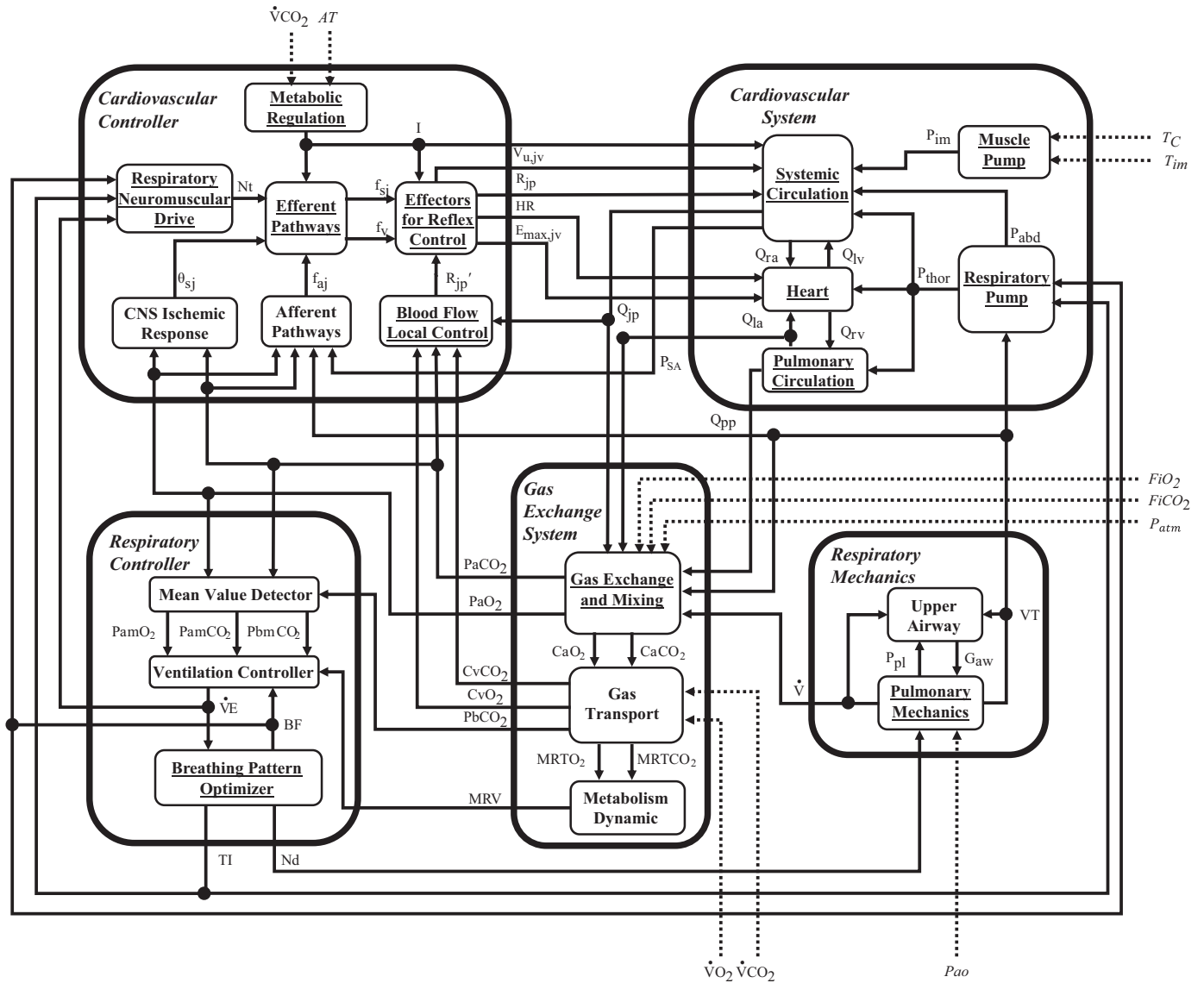
Figure 1. Model schematic block diagram. Dashed lines are inputs to the model. Blocks with underlined names correspond to the mechanisms added or are related to modifications made in this work. See Table 2 for symbols description. The mathematical equations of all systems and controllers are given in the Supplemental Material.

veins. Systemic circulation comprises blood circulation through the systemic arteries, peripheral vessels, systemic veins, and vena cava. Both peripheral and venous circulations are divided into five compartments, arranged in parallel, representing the blood circulation into the skeletal muscle, brain, coronary, splanchnic, and extra-splanchnic vascular beds.

In order to obtain a suitable model for the moderate aerobic exercise simulation, modifications based on the work of Magosso and Ursino (16) were applied. The added mechanisms included a separate description of vascular beds of active and resting skeletal muscles, the effect of muscular contractions on venous return, and the effect of respiration on the venous return of compartments located inside the thoracic and abdominal cavities. The addition of the active skeletal muscle compartment involves a division of the peripheral and venous circulation into six compartments arranged in parallel and includes regulatory mechanisms

that relate their pressure, resistance, volume, and flow during rest and exercise. During exercise, the resistance of the venous vascular beds of the active muscles (R_{amv}) differs from the other beds since it adopts a behavior inversely proportional to the total volume of blood it contains (V_{Tamv}) (see *Eq. 3*). Muscle contractions during exercise intervene in the venous return of active muscles due to their effect on the extravascular pressure (P_{im}), which adopts an oscillatory rhythmic behavior between zero and a positive value (see *Eqs. 4* and *5*). Concerning to the above, the pressure-volume relationship of the active muscular veins differs from the other vascular beds considering that the muscular contractions induce a negative transmural pressure, which, in turn, promotes its collapse and, therefore, a significant expulsion of blood volume. It is represented by a nonlinear relationship of collapsing tubes (see *Eq. 6*). The effect of respiration under exercise on the systemic circulation was included as the

Table 2. *Symbols' description of the block diagram of CR1*

Abbreviation	Description
$CaCO_2$	Carbon dioxide concentration in the arterial blood
CaO_2	Oxygen concentration in the arterial blood
$CvCO_2$	Carbon dioxide concentration in the venous blood
CvO_2	Oxygen concentration in the venous blood
$E_{max,jv}$	Regulated end-systolic elastance of each ventricle
f_{aj}	Afferent activity from arterial baroreceptors, chemoreceptors, and lung-stretch receptors
$FiCO_2$	Inspired fractions of dry carbon dioxide
FiO_2	Inspired fractions of dry oxygen
f_{sj}	Activity in efferent sympathetic fibers directed to arterioles, veins, and heart
f_v	Efferent vagal activity
G_{aw}	Airway flow gain factor
I	The action of central command
MRT_{CO_2}	Tissue/carbon dioxide metabolic ratio
MRT_{O_2}	Tissue/oxygen metabolic ratio
MRV	Metabolically related neural drive component to the ventilation
Nd	Neural drive signal
Nt	Central respiratory neuromuscular drive response
P_{abd}	Abdominal pressure
Pam_{CO_2}	Mean value of Pa_{CO_2} in each respiratory cycle
Pam_{O_2}	Mean value of Pa_{O_2} in each respiratory cycle
Pao	Pressure at the airway opening
Pb_{CO_2}	Brain carbon dioxide partial pressure
Pbm_{CO_2}	Mean value of Pb_{CO_2} in each respiratory cycle
P_{im}	Intramuscular pressure
P_{pl}	Intrapleural pressure
P_{sa}	Systemic arterial pressure signal
P_{thor}	Intrathoracic pressure
Q_{jp}	Blood flow of each peripheral compartment
Q_{la}	Cardiac input to the left atrium
Q_{lv}	Cardiac output from left ventricle
Q_{pp}	Cardiac output from the pulmonary peripheral compartment
Q_{ra}	Cardiac input to the right atrium
Q_{rv}	Cardiac output from left ventricle
R_{jp}	Regulated resistance of each peripheral compartment
R'_{jp}	Regulated resistance by the blood flow local control for each peripheral compartment
T_C	Overall duration of the muscular contraction
T_{im}	Time duration of the muscular contraction-relaxation cycle
$V_{u,jv}$	Regulated unstressed volume of each venous compartment
θ_{sj}	Offset term representing the effect of the CNS ischemic response on the sympathetic fibers directed to peripheral circulation, veins, and heart

action of the abdominal pressure (P_{abd}) and intrathoracic pressure (P_{thor}) (extravascular pressures) on the heart, lungs, and systemic veins, considering them as functions related to inspiratory and expiratory time, BF, and VT (see *Eqs. 7–10*):

$$R_{amv} = k_{r,am}/V_{Tamv} \quad I > 0 \tag{3}$$

where I is the relative intensity of aerobic exercise; R and V denote hydraulic resistance and blood volume, respectively; the subscript amv indicates the venous vascular bed of the active skeletal muscle, the subscript T indicates total value, and $k_{r,am}$ is a constant parameter.

$$P_{im} = A_{im} \cdot \psi(t) \tag{4}$$

$$\psi(t) = \begin{cases} \sin\left(\pi \cdot \dfrac{T_{im}}{T_C} \cdot \alpha\right) & 0 \le \alpha \le \dfrac{T_C}{T_{im}} \\ 0 & \dfrac{T_C}{T_{im}} \le \alpha \le 1 \end{cases} \tag{5}$$

$$P_{amv} = P_0 \cdot \left[1 - \left(\frac{V_{Tamv}}{V_{u,amv}}\right)^{-3/2}\right] + P_{im} \quad V_{Tamv} < V_{u,amv} \tag{6}$$

where P denotes pressure; $\psi(t)$ is the activation function of skeletal muscle fibers [with $\psi(t) = 1$ at maximum contraction, $\psi(t) = 0$ at complete relaxation]; α is a dimensionless variable, ranging between 0 (conventionally corresponding to the beginning of contraction) and 1, which represents the fraction of the muscle contraction-relaxation cycle; A_{im}, T_C, and T_{im} are parameters corresponding to the peak value of intramuscular pressure, the overall duration of muscular contraction and duration of the muscular contraction-relaxation cycle, respectively; the subscript im indicates the intramuscular circulation; the subscript u is used to indicate unstressed values; and P_0 is a constant parameter.

$$P_{thor}(t) = \begin{cases} P_{thormax} - (P_{thormax} - P_{thormin}) \cdot \dfrac{T_{resp}}{TI} \cdot S \ \ 0 \leq S \leq \dfrac{TI}{T_{resp}} \\[2ex] P_{thormax} - (P_{thormax} - P_{thormin}) \cdot \dfrac{(TI + TE - T_{resp} \cdot S)}{TE} \ \ \dfrac{TI}{T_{resp}} \leq S \leq \dfrac{TI + TE}{T_{resp}} \\[2ex] P_{thormax} \ \ \dfrac{TI + TE}{T_{resp}} \leq S \leq 1 \end{cases}$$

$$(7)$$

$$P_{abd}(t) = \begin{cases} P_{abdmax} - (P_{abdmax} - P_{abdmin}) \cdot \dfrac{T_{resp}}{TI/2} \cdot S \ \ 0 \leq S \leq \dfrac{TI/2}{T_{resp}} \\[2ex] P_{abdmin} \ \ \dfrac{TI/2}{T_{resp}} \leq S \leq \dfrac{TI}{T_{resp}} \\[2ex] P_{abdmax} - (P_{abdmax} - P_{abdmin}) \cdot \dfrac{(TI + TE - T_{resp} \cdot S)}{TE} \ \ \dfrac{TI}{T_{resp}} \leq S \leq \dfrac{TI + TE}{T_{resp}} \\[2ex] P_{abdmax} \ \ \dfrac{TI + TE}{T_{resp}} \leq S \leq 1 \end{cases}$$

$$(8)$$

$$P_{jmax} = P_{jmax,n} + g_j \cdot \Delta VT \tag{9}$$

$$P_{jmin} = P_{jmin,n} - g_j \cdot \Delta VT \tag{10}$$

where T_{resp} is the respiratory period; TE is the expiration time; $P_{thormin}$ and P_{abdmin} denote the values of intrathoracic and abdominal pressure at the end of inspiration; $P_{thormax}$ and P_{abdmax} are the values of the intrathoracic and abdominal pressures at the end of expiration and during the respiratory pause; S is a dimensionless variable ranging between 0 and 1, which represents the fraction of the respiratory cycle; ΔVT is the change in tidal volume induced by exercise; g is a constant gain factor related to tidal volume changes; the subscript j indicates the compartment abdominal (abd) and the extravascular of the active muscle veins (thor); and the subscript n denotes nominal values.

This model does not implement the description of the thoracic cavity proposed by Magosso and Ursino (16). Instead, the vena cava flow and pressure descriptions implemented by Cheng et al. (22) and based on the work proposed by Lu et al. (12) were included.

Cardiovascular controller.

The cardiovascular controller implemented is also largely based on the work by Ursino and Magosso (24) and Magosso and Ursino (23). It includes the blood flow local control, central nervous system ischemic response, the afferent pathways, the efferent neural pathways, and the cardiovascular effectors for reflex control. The blood flow local control comprises the vasodilatory effect on the cerebral, coronary, and skeletal muscle (active and passive) vascular beds in response to arterial oxygen and carbon dioxide. The central nervous system ischemic response corresponds to the effect of hypoxia on heart rate and systemic circulation, acting on the cardiac and peripheral sympathetic nerves. The afferent pathways comprise the action of carotid sinus baroreceptors, peripheral chemoreceptors, and lung stretch receptors. The afferent and central nervous system ischemic responses are first processed at the level of the autonomic nervous system in the efferent neural pathways, where the sympathetic and parasympathetic activities are modulated. Finally, the sympathetic and parasympathetic activity in the cardiovascular effectors, coming from efferent pathways and local regulation, regulate the heart period, maximum ventricular

contractilities, resistance of the systemic peripheral beds, and systemic venous unstressed volumes.

Mechanisms related to response to aerobic exercise were included in this controller. These mechanisms comprise the effect of respiration on sympathetic and parasympathetic activity proposed by Cheng et al. (22), the action mechanism of central command proposed by Magosso and Ursino (16), and a functional description of local metabolic vasodilation into active muscles. The effect of respiration through the central respiratory neuromuscular drive, arising from the respiratory centers and modulated by the respiratory autorhythmicity and ventilatory demand, influences the response in the efferent pathways through a directly proportional effect on sympathetic activity and inversely proportional effect on parasympathetic activity (see *Eqs. 11* and *12*). The central command mechanism evaluated as the metabolic regulation response, determined as a function of the *AT* and CO_2 production values at both rest and exercise, has a direct additive effect on the effector pathways, exciting the sympathetic activity and inhibiting the parasympathetic activity (see *Eqs. 13* and *14*) and an indirect vasodilator effect in response to the absence of oxygen and metabolic changes over the systemic peripheral vessels related to the active skeletal muscles (see *Eq. 15*).

$$Nt = \int_0^{TI} (\dot{V}E \cdot RR) dt \tag{11}$$

$$RR = \begin{cases} 1 & t < TI \\ 0 & TI \leq t \leq T_{resp} \end{cases} \tag{12}$$

where Nt is the central respiratory neuromuscular drive response and RR represents the respiratory rhythm.

$$I = \frac{(MRTCO_2 - MRTCO_2 basal)}{(AT - MRTCO_2 basal)} \tag{13}$$

$$\gamma_i = \frac{\gamma_{i,min} + \gamma_{i,max} \cdot \exp\left(\frac{1 - I_{0,i}}{k_{cc,i}}\right)}{1 + \exp\left(\frac{1 - I_{0,i}}{k_{cc,i}}\right)} \tag{14}$$

where $MRTCO_2$ *basal* is the value of basal metabolic production rate for CO_2 in tissues; γ is an additive term included in the expressions of sympathetic and parasympathetic activity to relate the action of the central command; I_0 and k_{cc} are constant parameter values; the subscript i = sp, sv, and sh indicates sympathetic activity to peripheral arteries, veins, and heart, and v denotes vagal activity; and the subscripts min and max denotes lower or higher saturation levels.

$$R_{amp} = \frac{R_{amp,n}}{(1 + x_{am,O_2} + x_{met})} \tag{15}$$

where $x_{am,O2}$ and x_{met} are state variables that represent the effect of tissue hypoxia and of the other vasodilatory substances, respectively, and the subscript p indicates peripheral vascular compartment.

Although the activity of afferent chemoreceptors by Magosso and Ursino in (16) was not incorporated based on the consideration that Pa_{O2} and Pa_{CO2} exhibit insignificant variations during aerobic exercise, in the present work their

action was implemented in accordance with Ursino and Magosso [24].

Respiratory mechanics.

The model of respiratory mechanics is largely based on the adaptation of the model by Cheng et al. [22] made in the study by Serna et al. [21]. It comprises two compartments representing the pulmonary and upper airway mechanics. The modifications were implemented in the pulmonary mechanics, specifically in the muscle pressure wave and the air movement equation. The implemented muscle pressure equation is the one proposed by Poon et al. [14], which is modeled as a quadratic function during inspiration and an exponential function during expiration (see *Eq.16*). The parameter values that define these waveforms are the result of respiratory controller regulation and are received in this system as an input named neural drive response (Nd) (see *Respiratory controller*). The volume and airflow signals are related to the muscle pressure signal according to the air movement equation proposed by M. Younes and W. Riddle [36–38]:

$$P_{musc}(t) = \begin{cases} a_0 + a_1 \cdot t + a_2 \cdot t^2 & 0 \leq t \leq t_1 \\ P_{musc}(t_1) exp^{(-(t-t_1)/tau)} & t_1 \leq t \leq t_1 + t_2 \end{cases} \quad (16)$$

where $P_{musc}(t)$ is the muscle pressure signal and a_0, a_1, a_2, t_1, t_2, and tau are the parameters resulting from the respiratory controller regulation that define the respiratory waveforms. They are received in this system as an input named neural drive response (Nd). $P_{musc}(t_1)$ is the peak inspiratory pressure at time t_1.

Respiratory controller.

The respiratory controller implemented in the proposed model is based on the adaptation of the model by Fincham and Tehrani [15] made in the study by Serna et al. [21], where the information provided by the central chemoreceptors ($Pmbco_2$), peripheral chemoreceptors ($Pamo_2$ and $Pamco_2$), and the metabolically related neural drive component to the ventilation (MRV) is used to estimate the ventilatory demand of the subject (i.e., the needed ventilation to keep arterial blood gases around their basal values; see *Eqs. 17* and *18*). MRV represents the neurogenic mechanism of the respiratory control system during exercise, which is received in this controller as an input, and it is a result of the gas exchange system (see *Gas exchange system*):

$$\dot{V}A = \dot{V}A_{rest} \cdot (KpCO_2 \cdot PamCO_2 + KcCO_2 \cdot PmbCO_2 + G_3 + KcMRV \cdot MRV - Kbg) \quad (17)$$

$$G_3 = \begin{cases} KpO_2 \cdot (104 - PamO_2)^{4.9} & PamO_2 < 104 \\ 0 & PamO_2 \geq 104 \end{cases} \quad (18)$$

where $\dot{V}A$ and $\dot{V}A_{rest}$ are the alveolar ventilation and its basal value, respectively; $Pamo_2$, $Pamco_2$ and $Pbmco_2$ are the mean values of Pao_2, $Paco_2$, and $Pbco_2$ in each respiratory cycle; $Kpco_2$, $Kcco_2$, Kpo_2, and $KcMRV$ are constant gain parameters for each receptor; and Kbg is the blood gas dissociation constant.

Instead of Otis' optimization approach [39], from which BF is calculated based on a steady-state minimization of

work of breathing (WOB) principle in [21], CR1 incorporates the optimization approach formulated in Serna Higuita et al. [40], wherein breathing pattern is adjusted at each cycle for a specific level of ventilation (set point) by minimizing cycle-cycle WOB (see *Eqs. 19–24*). It includes dynamic elements to relate the neural activity with ventilatory mechanics (i.e., neuromechanics efficiency factors) [36–38], and it distinguishes between the respiratory mechanical work carried out during inspiration ($\dot{W}_I$) and expiration ($\dot{W}_E$). So, it does fit not only the ventilation but also those variables associated with the overall breathing pattern, VT, BF, TI and TE.

$$\dot{W}_T = \dot{W}_I + \lambda_2 \cdot \dot{W}_E \quad (19)$$

$$\dot{W}_I = \frac{1}{(t_1 + t_2)} \int_0^{t1} \left[\frac{P_{musc}(t)}{\xi_1^n \xi_2^n} + \lambda_1 \cdot \ddot{V}(t)^2 \right] dt \quad (20)$$

$$\dot{W}_E = \frac{1}{(t_1 + t_2)} \int_{t1}^{t1+t2} \ddot{V}(t)^2 dt \quad (21)$$

$$Nd = [a_0, a_1, a_2, tau, t_1, t_2] \quad (22)$$

$$TI = t_1 \quad (23)$$

$$BF = 1/(t_1 + t_2) \quad (24)$$

where $\dot{W}_T$ represents the total mechanical work; $\dot{W}_I$ is mechanical work of the inspiratory phase; $\dot{W}_E$ is mechanical work of the expiratory phase; ξ_1 and ξ_2 are efficiency factors; Nd is the neural drive signal, which defines the breathing pattern subject; λ_1 and λ_2 are weighting factor; and n is a parameter that denote power index of efficiency factor.

For a respiratory cycle, the total mechanical work ($\dot{W}_T$) is formulated as a weighting sum of $\dot{W}_I$ and $\dot{W}_E$. $\dot{W}_I$ and $\dot{W}_E$ are represented as defined integrals, depending on muscle pressure [P(t)], respiratory volume [V(t)], and airflow [$\dot{V}(t)$] waveforms. Specifically, $\dot{W}_I$ is defined as an integral of a weighting sum between two components, the first one related to the product of P(t) and $\dot{V}(t)$ and the second one related to airflow rate, $\ddot{V}(t)$. Additionally, the first component is divided by efficiency factors that allow for considering the effects of respiratory-mechanical limitation, the decreases of neuromechanics efficiency with increasing respiratory efforts [14, 37, 41], and the non-linear variation of such as efficiencies. $\dot{W}_E$ is defined as an integral of $\ddot{V}(t)$. Physio-logical reasons that motivated to formulate such as works are mainly related to the respiratory muscles control, i.e., minimizing the oxygen consumption during ventilation and avoiding harmful effects related to high-pressure airflow rates [14, 41].

The two weighting factors of WOB and the nonlinear variation of mechanical plant efficiency are controller parameters that should be estimated by fitting techniques that guarantee a proper breathing pattern prediction (i.e., a good adjustment to experimental data). Taking into account the features of the patients under study (healthy subjects under exercise stimulus), the parameter values published by Serna Higuita et al. [40] were considered in this study. Therefore, the respiratory controller is formulated as an optimal controller minimizing $\dot{W}_T$ by optimizing those parameters defining

the respiratory waveforms. The same procedure used by Serna Higuita et al. (40) for the breathing pattern optimization was used in this work, so it is not detailed herein by brevity. A detailed description of relationships described above is provided in the Supplemental Material; subsection 4.2 (Supplemental Material for this article can be found online at https://doi.org/10.6084/m9.figshare.13107500).

Gas exchange system.
The gas exchange system of the present model is broadly based on the work proposed by Serna et al. (21). It consists of an adaptation of the work of Cheng et al. (22) that includes a separate description of the oxygen consumption and CO_2 production in both brain and tissues, a detailed description of the gas exchange at the cerebral level, and the determination of the dead space volume as a function of the alveolar flow. The cardiovascular system and respiratory mechanics interact through this system in order to regulate the concentration of blood gases. This system includes mechanisms related to the identification of dead space gas pressures, pulmonary gas exchange, mechanisms of mixing, convection, and dissociation of blood gas, and transport and exchange of blood gas in both brain and tissue levels. Regarding the exercise, it also integrates a mechanism for the identification of the metabolic rate ratio that relates the level of exercise regarding the $MRTCO_2$ and $MRTO_2$ values, which are necessary for the respiratory regulation (see *Eqs. 25–28*).

$$M'RR = \frac{(MRBCO_2 + MRBO_2 + MRTCO_2 + MRTO_2)}{(MRBCO_2 + MRBO_2 + MRTCO_2 basal + MRTO_2 basal)}$$
(25)

$$MRR = \begin{cases} M'RR & M'RR \geq 1 \\ 1 & M'RR < 1 \end{cases}$$
(26)

$$\tau MRV \cdot \frac{dM'RV}{dt} = (MRR - 1) - M'RV$$
(27)

$$MRV = \begin{cases} M'RV & M'RV \geq 0 \ \& \ MRR > 1 \\ 0 & M'RV < 0 \ | \ MRR \leq 1 \end{cases}$$
(28)

where MRR is the metabolic rate ratio and MRV is the metabolically related neural drive component to ventilation. $MRBCO_2$ and $MRBO_2$ are the metabolic production and consumption rate for CO_2 and O_2 in the brain tissue, respectively; $MRTO_2$ *basal* is the value of basal metabolic consumption rate for O_2 in tissues; τMRV is a metabolic rate time constant.

Modifications of the cardiac output were made in order to obtain more realistic results of the transport and exchange of blood gases in the brain and tissues. Instead of assigning a total cardiac output percentage to the brain and tissue perfusion ($0.85Q_{pp}$ and $0.15Q_{pp}$, respectively), the specific blood flow signals of the tissues and the brain were taken directly from the cardiovascular system to be used in the gas transport compartments (see Q_{jp} and Q_{pp} in Fig. 1). In this way, Q_{bp} is used to calculate the brain venous blood pressure of CO_2 ($PvbCO_2$; see *Eq. 29*) and the blood flow in the tissues (Q_T) the values of venous blood concentrations for CO_2 and O_2 ($CvCO_2$ and $CvCO_2$, respectively) (see *Eqs. 30–32*).

$$SbCO_2 \cdot \frac{dPvbCO_2}{dt} = MRBCO_2 + Q_{bp} \cdot SCO_2(PaCO_2 - PvbCO_2) - h$$
(29)

$$Q_T = Q_{pp} - Q_{bp}$$
(30)

$$VTCO_2 \cdot \frac{dCvCO_2}{dt} = MRTCO_2 + Q_T(CaCO_2 - CvCO_2)$$
(31)

$$VTO_2 \cdot \frac{dCvO_2}{dt} = -MRTO_2 + Q_T(CaO_2 - CvO_2)$$
(32)

where $SbCO_2$ is the dissociation slope for CO_2 in the brain tissue; SCO_2 is the dissociation slope for CO_2 in the blood; h is the cerebral blood flow constant; and $VTCO_2$ and VTO_2 are the body tissue storage volume for CO_2 and O_2, respectively.

Parameter Assignment

This section describes how the parameter values of the model CR1 were assigned in order to correctly adapt the different integrated systems, controllers, and mechanisms. The parameter values were mostly taken from each of the models on which the systems and controllers are based, except for some modifications associated with the exercise mechanisms included, which are described below for each system and controller.

All of the parameters discussed below have been assigned with reference to the characteristics of the same subject represented by the models on which it is based (a healthy subject of ~70 kg), and the values modifications were aimed at achieving the equivalence. Only the parameter values related to the main changes are presented in this section. The complete list of model parameters, the values used, and their descriptions are given in the Supplemental Material.

Cardiovascular system parameters.
The parameter values of the cardiovascular system, corresponding to resistances, compliances, and unstressed volumes, have been taken mainly from the model reported by Cheng et al. (22), but some of them were modified due to the addition of the active skeletal muscle compartments. This distinction between passive and active muscle compartments was applied in the work by Magosso and Ursino (16) and aims to evaluate the effect of the local vascular control processes of the muscles during exercise on the cardiovascular response (see the reference work for more details). The modifications were made in accordance with the conservative strategy proposed by Magosso and Ursino (16), where, considering that the characteristics of resistance, compliance, and unstressed volumes for the subject represented by the model do not vary with respect to those previously reported by Cheng et al. (22) and Serna et al. (21), the values of the parameters related to these characteristics in each compartment are calculated according to the proportion represented. The modified parameter values regarding the work by Cheng et al. (22) can be found in Table 3.

Cardiovascular controller parameters.
The parameter assignment of the cardiovascular control system depends on each included mechanism. The parameter values are taken mostly from work by Cheng et al. (22). Those related to the central command mechanism are taken

Table 3. *Parameters of the cardiovascular system*

Unstressed Volume, mL	Hydraulic Resistance, mmHg·s/mL	Compliance, mL/mmHg
$V_{u,amp}$ = 63.48	$R_{amp,0}$ = 3.51	C_{amp} = 0.315
$V_{u,rmp}$ = 42.3	$R_{rmp,0}$ = 5.27	C_{rmp} = 0.21
$V_{u,amv0}$ = 301.96	$R_{amv,n}$ = 0.0833	C_{amv} = 9.4
$V_{u,rmv0}$ = 201.30	$R_{rmv,n}$ = 0.125	C_{rmv} = 6.28
$V_{u,sv0}$ = 1435.4	$R_{sp,0}$ = 2.49	
$V_{u,ev0}$ = 640.73	$R_{ep,0}$ = 1.655	

$V_{u,amp}$ and $V_{u,rmp}$ are the peripheral unstressed volume in active and resting skeletal muscle; $V_{u,amv0}$, $V_{u,rmv0}$, $V_{u,sv0}$, and $V_{u,ev0}$ are the basal level of venous unstressed volume in active and resting skeletal muscle and splanchnic and extra-splanchnic circulation, respectively; $R_{amp,0}$, $R_{rmp,0}$, $R_{sp,0}$, and $R_{ep,0}$ are the peripheral resistance in active and resting skeletal muscle and splanchnic and remaining extra-splanchnic vascular beds, respectively; $R_{amv,n}$ and $R_{rmv,n}$ are the venous resistance in active and resting skeletal muscle, respectively; c_{amp} and c_{rmp} are the peripheral compliance in active and resting skeletal muscle, respectively; c_{amv} and c_{rmv} are the venous compliance in active and resting skeletal muscle, respectively.

from the work by Magosso and Ursino (16). Some parameters value were taken from the work of Albanese et al. (20), considering its good performance to predict both heart rate and systemic arterial pressure. These values, which are related to the central nervous system ischemic response, the afferent pathways, and the efferent neural pathways, are based on the previous work by Ursino and Magosso (24) and Magosso and Ursino (23) or are the result of modifications made by these authors [see the reference work of Albanese et al. (20) for more details]. The values of $W_{p,sv}$ and $W_{b,sv}$ were assigned maintaining the equality relation proposed by Cheng et al. (22) and Magosso and Ursino (23) regarding the values of $W_{p,sp}$ and $W_{b,sp}$. Table 4 shows the values of parameters taken from the work of Albanese et al. (20).

Respiratory mechanics parameters.

The parameter values of the respiratory mechanics largely have been taken from Serna et al. (21), using for the overall resistance (R_{rs}) and elastance (E_{rs}) the healthy people values

Table 4. *Parameters of the cardiovascular controller*

Central Nervous System Ischemic Response		
$k_{isc,sh}$ = 6 mmHg	x_{sh} = 53 spikes/s	
Afferent pathway		
G_{ap} = 11.76 spikes·L^{-1}·s^{-1}		
Efferent pathways		
$W_{c,sp}$ = 1.716	$W_{p,sp}$ = −0.3997	$W_{b,sp}$ = −1.1375
$W_{c,sv}$ = 1.716	$W_{p,sv}$ = −0.3997	$W_{b,sv}$ = −1.1375
$W_{c,sh}$ = 1	$W_{p,sh}$ = 0	$W_{b,sh}$ = −1.75
$W_{c,v}$ = 0.2	$W_{p,v}$ = −0.103	

$k_{isc,sh}$ is a gain parameter related to the heart sympathetic activity; x_{sh} is a saturation for the offset of heart sympathetic activity; G_{ap} is a constant gain related to the lung stretch receptors reflex; $W_{c,sp}$, $W_{c,sv}$, $W_{c,sh}$, and $W_{c,v}$ are the chemoreflex gain for the peripheral resistance, unstressed venous volume, heart sympathetic, and parasympathetic activity, respectively; $W_{p,sp}$, $W_{p,sv}$, $W_{p,sh}$, and $W_{p,v}$ are the lung stretch receptor reflex gain for the peripheral resistance, unstressed venous volume, heart sympathetic activity, and parasympathetic activity, respectively; $W_{b,sp}$, $W_{b,sv}$, and $W_{b,sh}$ are the carotid baroreceptor gain for the peripheral resistance, unstressed venous volume, and heart sympathetic activity, respectively.

Table 5. *Parameters of respiratory mechanics*

Resistance, cmH$_2$O·s/L	Elastance, cmH$_2$O/L
R_{rs} = 3.02	E_{rs} = 21.9
R_{CW} = 0.8326	E_{cw} = 10.545
R_L = 1.3661	E_L = 10.545
R_{AW} = 0.82128	

E_{CW}, chest wall elastance; E_L, lung transmural elastance; R_{AW}, airway wall resistance; R_{CW}, the chest wall resistance; R_L, lung transmural resistance.

reported by Poon et al. (14). According to this change, the compartment values (R_{CW}, R_L, R_{AW}, E_{cw}, and E_L) were calculated maintaining the proportion regarding the R_{rs} and E_{rs} values used in the Serna et al. (21) model. The modified values are shown in Table 5.

Respiratory controller parameters.

The parameter values of the respiratory controller correspond to those published by Serna et al. (40), specifically, those related to the weighting factors of the inspiratory and expiratory WOB, the respiratory efficiency factors, and their nonlinear variation (see Table 6). The efficiency factors allow for considering the effects of respiratory-mechanical limitation and the decreases of neuromechanics efficiency with increasing respiratory efforts (14). They depend on the parameters P_{max} and $\dot{P}_{max}$, whose values are those reported for a healthy subject in Serna Higuita et al. (40) and Poon et al. (14), respectively. Mathematical expressions relating them can be found in the Supplemental Material, subsection 4.2, Eqs. 145 and 146.

Gas exchange system parameters.

The parameter values of the gas exchange system correspond to those used by Serna et al. (21). Most of them are based on the work of Cheng et al. (22) and Fincham and Tehrani (15), but others were modified considering average values of the experimental data (see the reference work for more detail). Table 7 shows the values of the modified parameters in the work of Serna et al. (21).

Simulation

To evaluate whether CR1 is suitable to predict the cardiorespiratory response of a healthy human in rest and aerobic exercise, a comparison of model simulation results with two known cardiorespiratory models (20, 21) and experimental data was proposed. The experimental data corresponded to those obtained by the experimental test and the data processing described in this work (see *Experimental Design* and *Experimental Data Processing*). The models whose simulation results were compared are described below (see *Model*

Table 6. *Parameters of the respiratory controller*

Breathing Pattern Optimizer		
λ_1 = 0.860	λ_2 = 0.489	n = 1.101
P_{max} = 50 cmH$_2$O	$\dot{P}_{max}$ = 1000 cmH$_2$O/s	

λ_1 and λ_2 are weighing factors of the inspiratory and expiratory work; n defines the nonlinear variation of the mechanical plant efficiency; p_{max} is the maximum inspiratory muscle pressure; $\dot{P}_{max}$ is the maximum pressure rate during inspiration.

Table 7. *Parameters of the gas exchange system*

	Gas Exchange and Mixing	
$\beta_1 = 0.008275$		
	Gas Transport in the brain compartment	
$MRBCO_2 = 0.0009$ L/s STPD	$KCSFCO_2 = 320$ s	$h = 0.0183$ mL/(100 g·s)
$MRBO_2 = 0.000925$ L/s STPD	$KCCO_2 = 346000$ s·cm^{-2}·L^{-1}	$dc = 0.015$ cm
	Gas transport in body tissues compartment	
$VTCO_2 = 15$ L	$MRTCO_2 basal = 0.0033333$ L/s STPD	$MRCO_2 = 0.016667$ L/s STPD
$VTO_2 = 6$ L	$MRTO_2 basal = 0.0041667$ L/s STPD	$MRO_2 = 0.020833$ L/s STPD
$\tau MR = 50$ s		

β_1 is a parameter associated with the bohr and haldane effects regarding the O_2 dissociation in blood; $MRBCO_2$ and $MRBO_2$ are the metabolic production rate for CO_2 and O_2 in the brain tissue, respectively; $KCCO_2$ is the CO_2 central receptor constant; $KCSFCO_2$ is the CO_2 diffusion time constant of cerebrospinal fluid; h is the cerebral blood flow constant; d is the depth of central receptor below the surface of the medulla; $VTCO_2$ and VTO_2 are the body tissue storage volume for CO_2 and O_2, respectively; $MRTCO_2$ basal and $MRTO_2$ basal are the basal metabolic production rate for CO_2 and consumption rate for O_2, respectively; $MRCO_2$ and MRO_2 are the rates of production and consumption of CO_2 and O_2, respectively; τMR is the metabolic rate time constant; STPD is standard temperature and pressure, dry.

simulation results comparison). Considering the different specifications and constraints related to each model development, a standardization of the simulation conditions of all models was carried out. The simulation results were compared in both transient and steady state to verify the models' ability to predict the dynamics of the responses during stimulus transitions and once settling time has been achieved, respectively (see *Steady-state simulation* and *Transient simulation*). Because none of them consider the workload as a input variable, the simulation of the stimulus (rest and different levels of aerobic exercise) and the comparison with experimental data were performed considering the values of $\dot{V}O_2$ and $\dot{V}CO_2$ as reference (see *Inputs and standardization of simulation conditions*, *Steady-state simulation*, and *Transient simulation* for the description of the simulations and comparison in steady-state and transitory regime). Additionally, a sensitivity analysis was carried out to evaluate the individual role of each exercise mechanism included and adapted to the built model (see *Sensitivity analysis*).

The methodology implemented in this work is based on previous works of development, validation, and evaluation of physiological models (16, 18), among which the works of CR2 and CR3 are specifically included (1, 20, 21).

Model simulation results comparison.
The comparison between results of model simulation regarding experimental data was added to this work in order to *1*) evaluate that the integration and adaptation of the different systems, controllers, and mechanisms implemented were adequate and allowed the proposed model to predict the healthy human response in rest and aerobic exercise and *2*) analyze the differences and improvements of the built model, from a structural perspective, in regard to two of the most current and complete cardiorespiratory models validated under resting conditions. The implemented strategy is based on previous works of development, validation, and comparison of physiological models and contemplates quantitative and qualitative evaluations of the responses in steady state and transient regimen (1, 16, 18, 19, 21, 22).

The selection criteria of models to be studied were models comprising complete self-regulation of the cardiovascular and respiratory systems, models including variables resulting from the regulatory processes that correspond to those experimentally available, and models including at least the same processes and controllers of the evaluated model (CR1),

and they allow the simulation of aerobic exercise stimulus. The models of Albanese et al. (20) (CR2) and Serna et al. (21) (CR3), which correspond to two of the most current and complete cardiorespiratory models, were selected. A qualitative description of each model is presented below. The equations and parameters of each model will not be presented in this paper for reasons of brevity; the interested reader can refer to the referenced studies for details.

CR2 model. CR2 is an integrated model focused on a finer description of cardiorespiratory interactions and their respective control mechanisms (20). This model is based on previous models of different authors, highlighting mainly the works of Ursino and Magosso (24) and Magosso and Ursino (23) regarding the cardiovascular system and cardiovascular control. Its development and validation are based mainly on the analysis of hypercapnic and hypoxic stimuli, and it has been applied in works related to the estimation of respiratory work in a noninvasive way and studies of mechanical ventilation (42, 43).

The model can generate physiological variable values typically observed in adult humans under normal, hypercapnic, and hypoxic conditions. Although this model has not been fitted or validated to simulate aerobic exercise, it can be evaluated by the modification of parameter values related to metabolic rates. Some of its main features include the consideration of a pulmonary shunt in the cardiovascular and gas exchange systems, the inclusion of a thoracic vein compartment in the systemic circulation, the consideration of intrapleural pressure as a reference of extravascular pressure, the inclusion of chest-wall and pleural pressure dynamics in the respiratory system model, the description of gas exchange and venous gas transport for each systemic peripheral and venous compartments, and the inclusion of a more detailed afferent chemoreceptor pathway model (44).

CR3 model. CR3 is a cardiorespiratory model focused on the respiratory dynamics under the stimulus of moderate exercise (21). It is based mainly on the work by Cheng and Khoo (17), which corresponds to one of the most comprehensive cardiorespiratory models, widely validated and applied to simulate control dynamics during wakefulness and sleep. This model incorporates modifications adapted from the work by Fincham and Tehrani (15), related to a better response of the respiratory system, its controller, and the gas exchange plant under aerobic exercise stimulus.

CR3 was fitted and validated regarding experimental data of a cardiopulmonary exercise test, and its main feature consists of the incorporation of the adjustment of breathing pattern by using the optimization criteria set by Otis et al. (39).

Inputs and standardization of simulation conditions.
The simulation results of the models were evaluated considering different levels of exercise. The $\dot{V}O_2$ and $\dot{V}CO_2$ parameters were used as inputs to simulate the exercise stimulus. This choice is justified considering that the models evaluated do not incorporate the exercise workload as a possible input parameter, it has been shown that the metabolic rates of consumption and production of gases are directly related to the body's response during exercise, and its variation has been applied in different works for the simulation of this stimulus (14, 19, 45, 46). The $\dot{V}O_2$ and $\dot{V}CO_2$ simulated values correspond to experimental population values, all under normoxic conditions, applied in the gas exchange systems of each model, and considering that the input variations were only applied to organs different to the brain. Due to the specificity of the gas exchange system of CR2 with respect to CR1 and CR3, the simulated values of $\dot{V}O_2$ and $\dot{V}CO_2$ for this model in each organ were calculated in agreement with the respective proportion of the total CO_2 production and O_2 consumption reported by Albanese et al. (20).

Considering the different specifications and constraints related to the development of each model when they were designed and validated by their authors (characteristics of the population, the environmental conditions, and the stimulus of interest), a standardization of the simulation conditions for all models was carried out. In this procedure, focused on bringing the simulation conditions of the three models as close as possible to the experimental data used as reference, some parameters were replaced by data obtained from the cardiopulmonary exercise test (such as the average anthropometric data, associated with environmental conditions or characteristics of the experiment). None of the model parameters was adjusted or modified based on the output cardiorespiratory variables to be reproduced. The values of these model parameters were established in the current study in a similar way to how other authors have previously calculated and published with respect to other experimental data (13, 21). Some values were established considering the direct equivalence of the parameters with respect to the average characteristics of the experimental data, and others correspond to the application of previously reported and widely validated equations. Most of the modifications corresponded to common parameters among the three models, although there were also particular cases related to the structural characteristics of each one. The parameters that were not modified as part of the standardization, because they were not related to the available experimental measures, were equivalent to the nominal values reported for each model, which in the case of CR1 correspond to those presented in the Supplemental Material.

Parameters related to inspiratory gas fractions (FiO_2 and $FiOC_2$) and P_{atm} were selected considering the influence of environmental conditions, and their values were replaced by those registered experimentally. Parameters such as the basal respiratory tidal volume (VTn), basal metabolic rates, *mean AT*, inspiratory/expiratory time ratio at rest ($IEratio_n$),

total blood volume (V_{tot}), and constant unstressed values of blood volumes were selected considering the subjects' characterisics, and their values were modified by experimental measures or estimates derived from applying equations. The metabolic rates T_C and T_{im} were selected as parameters related to stimuli, and their values were replaced by experimentally recorded measurements. *VTn, mean AT, T_C,* and T_{im} are specific parameters for CR1 due to the adapted cardiovascular mechanisms effect on the cardiovascular system, and $IEratio_n$ was used only for the CR2 model to bring it closer to the experimental data, although this variable is not autoregulated, and its value remains constant.

The *mean AT* value was calculated using the procedure described in *Data restriction to aerobic exercise*. The total blood volume in milliliters was estimated as a function of the body surface area (BSA) in m^2 using *Eq. 34* (52). BSA was calculated as a function of the mean values of the height in centimeters and weight in kilograms using *Eq. 33* (53). The parameters related to the blood volumes in the models, corresponding to the unstressed volumes, were calculated as the proportion of the total blood volume as reported for each model.

$$\text{BSA} = \sqrt{\frac{(\text{Weigth} \cdot \text{High})}{3600}} \qquad (33)$$

$$V_{tot} = 1000 \ (3.29 \cdot \text{BSA} \ - \ 1.29) \qquad (34)$$

Steady-state simulation.
The steady-state models' performance was evaluated by calculating the prediction capability of each one regarding the steady-state experimental measurements of the cardiorespiratory variables. Variations of $\dot{V}O_2$ and $\dot{V}CO_2$ were simulated as eight consecutive, equidistant, and incremental steps from rest to moderate exercise, taking as a reference their respective mean experimental value from rest to *AT* (see the Tables 9 and 10). The simulation time for each step was 3,000 s, which was enough to guarantee the settling time of

Table 8. *Sensitivity and linearity results for cardiorespiratory variables under incremental exercise*

Variable	Slope ($\times 10^{-3}$)	Coefficient of Determination (%)
$\dot{V}CO_2$	20.4 ± 3.4	98.2 ± 1.1
$\dot{V}O_2$	17.1 ± 2.6	98.8 ± 0.8
$\dot{V}E$	16.5 ± 3.6	96.4 ± 2.3
VT	8.9 ± 2.4	95.3 ± 7.0
HR	5.2 ± 1.5	94.7 ± 16.4
BF	3.6 ± 1.8	71.4 ± 25.8
TI	2.3 ± 1.1	61.9 ± 32.1
PS	2.1 ± 0.8	86.8 ± 9.2
PM	1.2 ± 0.7	55.3 ± 29.7
PD	1.0 ± 0.8	36.3 ± 32.4
PA_{O_2}	0.6 ± 0.5	54.2 ± 34.3
PA_{CO_2}	0.3 ± 0.3	36.1 ± 30.0

Values shown correspond to the mean ± SD of the slope and coefficient of determination values as a function of the load of the cardiorespiratory variables for the 30 healthy subjects under the incremental exercise stimulus. BF, breathing frequency; HR, heart rate; PA_{CO_2}, alveolar partial pressure of CO_2; PA_{O_2}, alveolar partial pressure of O_2; PD, diastolic blood pressure; PM, mean arterial blood pressure; PS, systolic blood pressure; TI, inspiratory time; $\dot{V}CO_2$, carbon dioxide production; $\dot{V}E$, minute ventilation; $\dot{V}O_2$, oxygen uptake; VT, tidal volume.

Table 9. *Values of ventilatory and AT results*

Variable	Ventilatory Threshold	AT
$\dot{V}E$, L/min	41.0 ± 11.6	30.6 ± 9.0
$\dot{V}CO_2$, L/min	1.4 ± 0.4	1.0 ± 0.3
$\dot{V}O_2$, L/min	1.4 ± 0.4	1.1 ± 0.3

Values shown correspond to the mean ± SD of minute ventilation ($\dot{V}E$), carbon dioxide production ($\dot{V}CO_2$), and oxygen uptake ($\dot{V}O_2$) of the 30 subjects at which the ventilatory threshold and anaerobic threshold (*AT*) were reached under incremental exercise stimulus.

all the simulated variables in each model and covers the values reported by all authors. The model responses in steady state corresponded to the mean values of each variable at the last minute of each simulated input step.

Transient simulation.
The models' transient performance was evaluated through two simulation settings: first, using the simulation of three consecutive load steps, and second, using the simulation of a single load step. Both evaluations were performed varying $\dot{V}O_2$ and $\dot{V}CO_2$ variables according to experimental data and restricted to be below the *AT* of each subject. With the aim of comparing the subject's dynamic responses to exercise, simulation results are presented as percentage changes in the analyzed variables regarding their initial value. Systemic arterial pressures were not evaluated in this case because only their steady-state experimental values were available.

The first simulation aims to analyze in detail the models' predictions under the same conditions of the experimental test in the aerobic exercise range. The simulation inputs correspond to the continuous changes of the experimental values of $\dot{V}O_2$ and $\dot{V}CO_2$ for each subject between the end of the warming phase to the end of the third load step of the exercise phase. The total simulation time was 900 s and corresponded to the experimental duration of the evaluated load steps. The final prediction results of each model for each variable correspond to the average of the predictions performed for all subjects. The loading steps were selected considering that, in each step, all subjects are already prepared for the exercise, and most of them do not reach their *AT*.

The second simulation aims to analyze in detail the dynamics of the results under a load change, especially evaluating the time in which the predictions reach a steady state. Single steps of $\dot{V}O_2$ and $\dot{V}CO_2$ were simulated as inputs, varying their values between the respective experimental data at the beginning and at the end of the first load step of the exercise phase. The load step was selected considering that the subjects were already prepared for the exercise, and during this load most of them do not reach their *AT*. The simulated input values correspond to the mean experimental values of $\dot{V}O_2$ and $\dot{V}CO_2$ in the last minute at the end of the warming phase and at the end of the first load step of the exercise phase. The simulation time for the step was 3,000 s like in the steady-state simulation because it covers the settling time reported by all authors, even though the simulation time was longer than the experimental record, and the experimental inputs do not represent an ideal step input.

Sensitivity analysis.
Although each of the exercise mechanisms included have previously been validated, considering the differences between the models and conditions in which they were originally implemented, a sensitivity analysis was applied to compare the role and impact of each one in CR1. The sensitivity analysis allows for getting the percent changes of the CR1 predictions in response to an increase in stimulus from rest to a level of aerobic exercise, first when all mechanisms are intact and then after selective exclusion of a single mechanism. The variables, their measurements, and the simulation characteristics of the stimulus are the same as those evaluated for steady-state simulation, but only until reaching a $\dot{V}CO_2$ value of 0.7 L/min, equivalent to an intermediate stimulus level between rest and *AT*. The mechanisms evaluated correspond to those listed and described in the model development (see the *Model Building*). The action of the central respiratory neuromuscular drive (NT) and the central command (I-EP) on the sympathetic and parasympathetic efferent control activities and the neural driving component metabolically related to ventilation (MRV) were excluded by opening their corresponding feedback loop (see *Eqs. 11, 14,* and *17*). For the exclusion of the mechanisms associated with the separate description of the active muscles (V-R_{amv}), it was assumed that the behavior of R_{amv} did not vary with respect to the other vascular beds, depending on I (see *Eq. 3*). The effect of the muscle pump on venous return (MP) was excluded assuming that P_{im} is constant and equal to zero and that P_{amv} has the same behavior as venous pressure in the other venous vascular beds (see *Eqs. 4–6*). The effect of the respiratory pump (RP) was excluded considering the values of P_{abd} and P_{thor} constant and equal to the mean of their respective maximum and minimum reported nominal values (see *Eqs. 7–10*). The vasodilator action on active muscles due to the central command (I-R_{amp}) was excluded assuming that $x_{am,O2}$ does not vary as a function of I (remaining at its nominal value) and making x_{met} equals to zero (see *Eq. 15*). The effect of using blood flow signals from the cardiovascular system in the gas exchange system (Q-GES) was excluded assuming that cerebral and tissue perfusion correspond to a percentage of total cardiac output, as proposed in the base model (85% and 15%, respectively) (see *Eqs. 29–32*) (21). Finally, to exclude the respiratory control approach focused on minimizing the mechanical work of breathing (minWOB) and, therefore, the related respiratory mechanics (see *Eqs. 19–24* and *Eq. 16*), they were replaced by those originally proposed in the base model (21).

Computational Implementation and Data Analysis

All models were implemented in SIMULINK/MATLAB. The numerical solver and simulation characteristics used for the CR2 and CR3 models were the same reported in their respective works (20, 21). For CR1 and CR3, the Bogacki and Shampine BS23 algorithm for the solution of ordinary nonrigid differential equations was implemented (ODE23), and a variable step size between 1×10^{-2} s and 1×10^{-3} s was used. For CR2, the fourth-order Runge-Kutta method for numerical integration of the differential equations was implemented (ODE4), and a fixed-step size of 6×10^{-4} s was used.

The simulation of each model was run once, considering that none of them had stochastic characteristics.

The calculations applied to analyze the experimental data and to quantitatively assess the prediction capability and the dynamics of the models are described below.

Prediction error.

A comparison of every model prediction regarding each subject experimental data was evaluated quantitatively by the prediction error (PE) calculated from variables in steady state. The analyzed cardiorespiratory variables are the following:

- $\dot{V}E$, TI, VT, and BF, which provide information about the respiratory mechanics and controller,
- HR, PS, PD, and PM, which provide information about the cardiovascular system and controller,
- PA_{O_2} and PA_{CO_2}, which provide information about the gas exchange system.

PE was calculated by measuring the percentage differences between simulated results (sim) and experimental data (exp), using *Eq. 35* as follows:

$$\text{PE}(\%) = 100 \cdot \frac{1}{N} \sum_{j=1}^{N} \left(\text{Median}_{i,k} \left(\left| \frac{y_{\exp_{i,j,k}} - y_{\sim_{i,j,k}}}{y_{\exp_{i,j,k}}} \right| \right) \right)$$

$$(35)$$

where $y_{\exp}$ is the experimental variable value; $y_{\sim}$ is the simulation prediction value; N denotes the number of variables; and i, j, and k are indexes that represent each subject, variable, and stimulus level, respectively.

The metric presented is based on the measurement of the absolute mean error, and its selection obeys the following considerations. *1*) It allows the direct interpretation of the deviation from predictions as a proportion of the experimental data, and *2*) the application of the median allows for evaluating the trend of the results for the variables considering a nonnormal distribution regarding the population evaluated.

Settling time.

To assess the model's response speed to changes in their inputs, we measured the settling time of the analyzed variables for the single load step simulation. Its calculation consisted of finding the time for which the prediction varies less than ± 5% of the final simulated value.

Statistical analysis.

The results of the experimental data processing are presented as the mean value and its standard deviation. Nonparametric tests were used to identify statistical differences, with a significance level of $P \leq 0.05$. The Friedman test was implemented to identify differences between the model prediction error, and the Wilcoxon-Mann-Whitney test was used to identify the model with the best fitting to experimental data.

RESULTS

Experimental Data of Cardiopulmonary Exercise Test

Figure 2 shows the results of the cardiopulmonary exercise test. This figure shows the experimental data of the 30 registered subjects and their mean trend, detailing the different phases and loads applied regarding the time.

The following experimental behaviors in response to the increase in the level of exercise are mainly highlighted: *1*) relatively linear increases in $\dot{V}CO_2$ and $\dot{V}O_2$ with respect to the increase in load, similar to the results obtained in previous studies and which corroborate the use of these variables in past works as input signals for the simulation of the stimulus (14, 19, 26, 46); *2*) slight changes in PA_{CO_2} and PA_{O_2} which, according to previous studies (6, 7), are related to changes in blood gas concentrations and pressures and which attempt to be regulated by cardiovascular and respiratory changes; and *3*) increases in HR, PS, PM, BF, VT, and $\dot{V}E$ and decreases in TI, consistent with what is normally reported under exercise and which is related to the response of the cardiovascular and respiratory systems in an attempt to regulate gas exchange during exercise (6, 7).

Table 8 shows the results of the sensitivity and linearity of every variable. The obtained results allow for classifying the variables into three groups. The first group is formed by $\dot{V}CO_2$, $\dot{V}O_2$, $\dot{V}E$, VT, and HR, the variables with both the highest sensitivity to the exercise stimulus and the most linear behavior (coefficient of determination >90%), and the second group is formed by BF, TI, PS, PM, and PD, with lower slopes and coefficient of determination. Finally, the third group is formed by PA_{CO_2} and PA_{O_2}, the variables with the lowest slopes. Regarding the dispersion of the data, for the sensitivity results, in general, there is an opposite relationship with the magnitude of the calculated slope, allowing for classifying the variables in three groups similar to those previously described, whereas the linearity dispersion enables the classification of the variables into two groups: the first one formed by $\dot{V}CO_2$, $\dot{V}O_2$, $\dot{V}E$, and VT, corresponding to the variables having the lower dispersion values, and HR, BF, TI, PS, PM, PD, PA_{CO_2} and PA_{O_2} to those with higher dispersion values.

Table 9 presents the mean value and the standard deviation of *AT* and ventilatory threshold of $\dot{V}CO_2$, $\dot{V}O_2$, and $\dot{V}E$ obtained from the 30 subjects according to the algorithm of calculation implemented. Concerning the load, *AT* was reached between the second and third load step of the exercise phase for most subjects.

Simulation Results

Table 10 shows the inputs and parameter values calculated from the experimental data for setting the simulations. *FiO₂* and *FiCO₂* were calculated at atmospheric pressure of 640 mmHg using their corresponding partial pressure. Only the minimum common values of $\dot{V}CO_2$ and $\dot{V}O_2$ of the subjects are presented. The maximum values used for the simulations correspond to the results related to *AT* already presented. The used values of T_{im} and T_C were the same proposed by Magosso and Ursino (16).

Table 11 shows the parameter values calculated for the unstressed blood volumes. These results exhibited common parameters with similar values between the models. The main differences among them are presented in CR1, and they are related to the exercise mechanisms, mainly about the behavior of blood vessels in muscle compartments (see the *Cardiovascular system*).
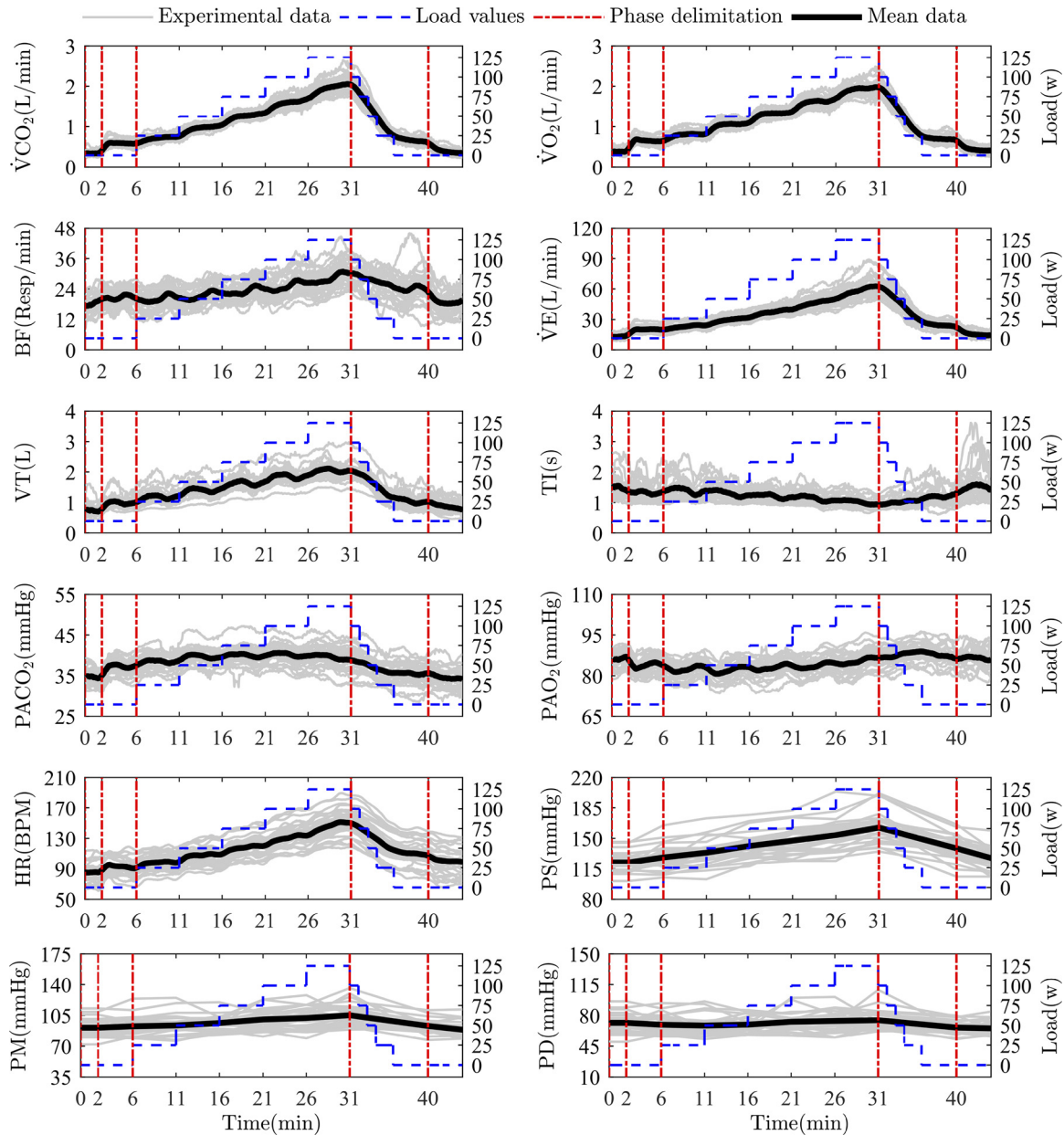
Figure 2. Experimental data distribution in function of time. For each variable, the solid gray lines are the experimental data; blue dashed lines are the load values, red dot-dashed lines are the phase delimitation times, and the solid black lines are the mean trend of the experimental data.

Steady-state response.

Figure 3 shows the steady-state results of the models' predictions for the $\dot{V}E$, VT, BF, TI, HR, PS, PM, PD, PA_{CO_2}, and PA_{O_2} variables when eight equidistant step inputs of $\dot{V}CO_2$, from 0.3 L/min to 1.0 L/min, were applied. It compares the models' prediction results with the experimental data restricted to AT of each subject and all subjects' averages.

The experimental results in steady state confirm the linear behavior of $\dot{V}E$ by increasing the exercise (28). Simulation results of all models have responses similar to those expected due to the increase in exercise, with some exceptions. In CR2, PA_{O_2} extremely differs from experimental data above 0.5 L/min $\dot{V}CO_2$. Moreover, most predictions show behaviors similar to first- or second- degree polynomial

relationships regarding the stimulus, except in PM, PS, and PD in CR1, whose dynamic cannot be approximated to such relationships. On the other hand, the CR1 predictions present the best fit to the experimental mean value for $\dot{V}E$, VT, TI, and PD; the CR3 predictions present the best fit to the experimental mean value for BF, HR, PS, PA_{CO_2}, and PA_{O_2}, and CR2 only has the best fit for PM.

Figure 4 shows the PE values obtained by each model and variable. The mean values, the median values, the interquartile range, and the statistically significant differences of the PE results for each models' predictions, with their respective overall PE value, are presented.

According to the PE results, the best predictions correspond to those obtained with CR1, followed by CR3 and

Table 10. *Values of inputs and parameters calculated from experimental data*

Environmental Conditions	
$FiO_2 = 21.0379$ %	$FiCO_2 = 0.0421$ %
Model Inputs	
$\dot{V}CO_2min = 0.30$ L/min	$\dot{V}O_2min = 0.33$ L/min
Additional Parameters	
$VTn = 0.73$ L	$V_{tot} = 5027.6$ mL
$T_{im} = 1$ s	$T_C = 0.75$ s
$IEratio_n = 0.8$	

Values of inputs and parameters calculated from experimental data, used for the simulation of the models.

finally by CR2. Specifically, CR1 obtained the lowest PE for V̇E, VT, TI, and PD; CR3 for BF, HR, PS, $PAco_2$, and PAo_2; and CR2 only for PM. All models showed statistically significant differences in the PE values of most variables. However, CR1 and CR3 obtained similar results for HR, BF, and PAo_2 with no significant difference, whereas PM and PS did not show any significant difference between any model pair. In terms of accuracy, CR1 and CR3 are the models with the closest predictions to most experimental data.

Table 12 shows the mean values and the standard deviation of PE for each model according to the related subsystem. These results indicate that CR1 has the highest accuracy and precision for all of its subsystems. The CR1 predictions were followed by CR3 and then by CR2, highlighting the closeness of the results between CR1 and CR3 regarding the gas exchange system and CR2 and CR3 regarding the cardiovascular system.

Transient response.
Figure 5 shows the transient response of the models' predictions for the simulation of continuous changes of the stimulus in real time corresponding to the first three exercise phase load steps. The results are presented as percentage changes regarding the final value of the warming phase. They are compared with the experimental data restricted to each *AT* for the respective load steps and their total mean value. It can be seen that CR1 presented the fastest dynamics and more similar and closer waveforms to experimental data, which was followed in order by CR3 and CR2. Individually, CR1 obtained the best results regarding the experimental mean value of HR, PAo_2, V̇E, and VT; CR2 got the best predictions for BF and TI, and CR3 the best one for PAo_2. The differences in the transient behavior evidenced for the models are related to the mechanisms that describe their dynamic cardiorespiratory response, which for CR1 are specifically related to the exercise stimulus, highlighting mainly the effects of the muscular and respiratory pump, the actions of central command, the approach of minimizing the breathing work, and the use of blood flow signals in the gas exchange system (see the *Model Building*). It is highlighted that none of the models adequately predict the dynamics of the experimental data related to BF and TI.

Figure 6 shows the model transient responses for a single step load simulation. The experimental data and models' predictions are presented as percentage changes

regarding their respective initial values. The experimental data, its mean value, and the models' results are compared in each variable, even though the simulation time was longer than the experimental record lasted, and the experimental inputs do not represent ideal step inputs (they depend on V̇CO₂ and not the workload). Experimental data are restricted to *AT*.

Transient simulation results show that CR1 has the highest response speed and the greatest similarity to experimental data, followed in order by CR3 and CR2. It is highlighted that the CR2 prediction for PAo_2 shows notably different behavior. Specifically, the CR1 predictions are the closest to experimental data for V̇E and HR, both in terms of shape and response speed, showing behavior similar to a first-order system. CR1 and CR3 present simulations that lightly follow the experimental values for VT, BF, TI, and $PAco_2$, although they do not correctly predict their dynamics. On the contrary, CR1 and CR3 present a dynamic response similar to experimental data for PAo_2, although they do not predict exactly the percentage change.

Table 13 shows the results of the settling time of every model's response to the single load step input. These results confirm that CR1 has the highest response speed for the cardiovascular and respiratory variables, followed in order by CR3 and CR2. It also highlights the slow response of all models to predict the gas exchange variables and that the simulation time for CR2 is not enough to reach the steady state of any variable.

Table 11. *Values of model parameters calculated from experimental data*

Unstressed Volume, mL	CR1	CR2	CR3
$V_{u,ep}$	127.72	127.72	127.72
$V_{u,sp}$	260.3	260.3	260.3
$V_{u,rmp}$	40.1	100.4	100.4
$V_{u,amp}$	60.22		
$V_{u,bp}$	68.42	68.42	68.42
$V_{u,hp}$	23	23	23
$V_{u,ev0}$	607.80	607.80	607.80
$V_{u,sv0}$	1,361.6	1,361.6	1,361.6
$V_{u,rmv0}$	190.95	477.39	477.39
$V_{u,amv0}$	286.4		
$V_{u,bv}$	279.49	279.49	279.49
$V_{u,hv}$	93.16	93.16	93.16
$V_{u,vc}$	123	123	123
$V_{u,ra}$	24	21	24
$V_{u,rv}$	38.703	34.058	38.703
$V_{u,la}$	24	21	24
$V_{u,lv}$	15.9080	13.9990	15.9080
$V_{u,pp}$	116.6775	100.9307	116.6775
$V_{u,pv}$	114.0	100.2	114.0

Values of unstressed volume parameters calculated from experimental data and used for the simulation of the models. $V_{u,ep}$, $V_{u,sp}$, $V_{u,hp}$, and $V_{u,bp}$ are the peripheral unstressed volume in extrasplanchnic, splanchnic, coronary, and brain circulation, respectively; $V_{u,ev}$, $V_{u,sv}$, $V_{u,hv}$, and $V_{u,bv}$ are the venous unstressed volume in extrasplanchnic, splanchnic, coronary, and brain circulation, respectively; $V_{u,vc}$ is the vena cava unstressed volume; $V_{u,ra}$, $V_{u,rv}$, $V_{u,la}$, and $V_{u,lv}$ are the unstressed volume in the right-atrium, right-ventricular, left-atrium, and left-ventricular circulation, respectively; $V_{u,pp}$ and $V_{u,pv}$ are the unstressed volume in the pulmonary peripheral and pulmonary veins circulation, respectively. Subscript 0 is used in the parameters that are subject to control mechanisms.
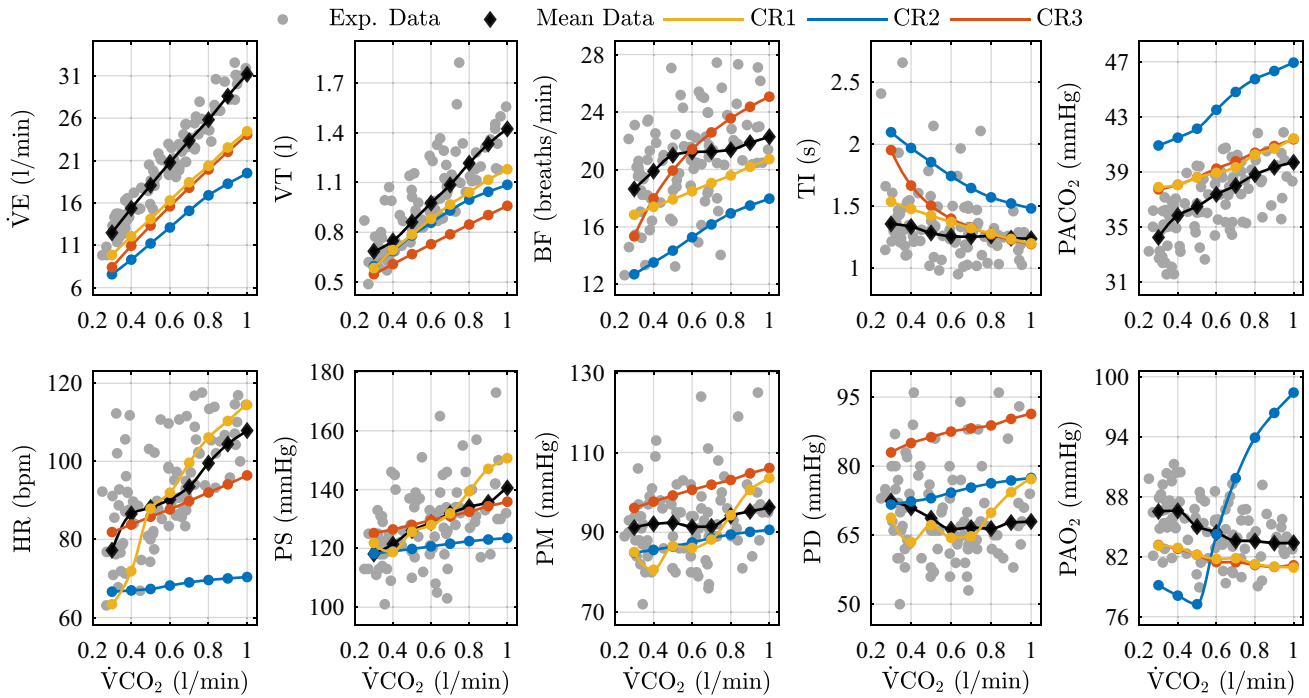
Figure 3. Steady-state simulation results in variations of $\dot{V}O_2$ and $\dot{V}CO_2$ as consecutive, equidistant, and incremental steps for ventilation ($\dot{V}E$), tidal volume (VT), breathing frequency (BF), inspiratory time (TI), alveolar partial pressure of CO_2 (PA_{CO_2}), alveolar partial pressure of O_2 (PA_{O_2}), heart rate (HR), systolic blood pressure (PS), diastolic blood pressure (PD), and mean arterial blood pressure (PM). The results are shown as a function of $\dot{V}CO_2$ values, corresponding to simulated step input values from 0.3 to 1 L/min. For each variable, gray dots are the experimental data restricted by each subject's *AT*, black dots and lines are the average of the experimental data, yellow dots and lines are predictions of CR1, blue dots and lines are the predictions of CR2, and orange dots and lines are predictions of CR3.

Sensitivity analysis results.

Figure 7 shows the results of sensitivity analysis for the CR1 model. The variations obtained by selectively excluding a single mechanism are presented as the percent changes of each variable. The simulation conditions regarding the exclusion of the mechanisms are as follows: all mechanisms intact (all-included), exclusion of central command action on sympathetic and parasympathetic efferent control activities (I-EP excluded), exclusion of the action of the central respiratory neuromuscular drive on the sympathetic and parasympathetic efferent control activities (NT Excluded), exclusion of vasodilatory action on active muscles due to central command (I-R$_{amp}$ excluded), exclusion of mechanisms associated with a separate description of venous vascular beds from active muscles (V-R$_{amv}$ excluded), exclusion of the muscle pump mechanism (MP excluded), exclusion of the respiratory pump mechanism (RP excluded), exclusion of the neural driving component metabolically related to
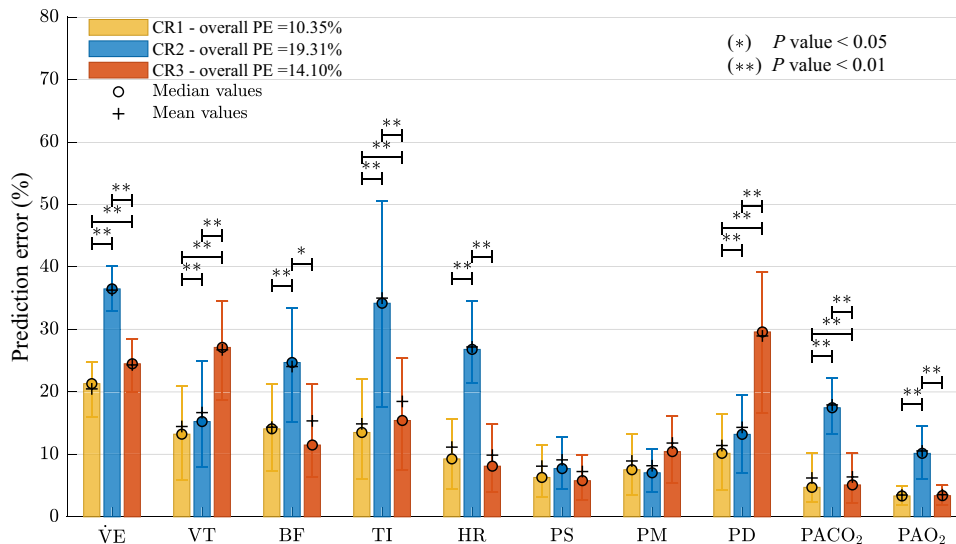

Figure 4. Prediction error (PE) results of the evaluated models for the steady-state simulation. Bar graph shows median values, and error bars indicate interquartile distance (range of values from 25 to 75% quartile). For each variable, yellow bars correspond to CR1 results, blue bars correspond to CR2 results, and orange bars correspond to CR3 results. Statistically significant differences between the obtained PE values were found using the Wilcoxon signed-rank test. *$P < 0.05$; **$P < 0.01$.

Table 12. *Prediction error (%) for each cardiorespiratory subsystem*

Model	Cardiovascular	Respiratory Mechanics	Gas Exchange
CR1	8.33 ± 1.73	15.54 ± 3.87	4.03 ± 0.97
CR2	13.70 ± 9.16	27.66 ± 9.72	13.82 ± 5.16
CR3	13.49 ± 10.91	19.64 ± 7.39	4.26 ± 1.22

The shown values correspond to the mean and the SD of prediction error for each model in the variables related to the cardiovascular, respiratory mechanics, and gas exchange subsystem working in close loop.

ventilation (MRV Excluded), exclusion of the respiratory control approach focused on minimizing the mechanical work of breathing (minWOB excluded), and exclusion of the use of blood flow signals from the cardiovascular system in the gas exchange system (Q-GES excluded).

According to expectations, considering the specificity of each mechanism with respect to the systems or controllers of the model, the selective exclusion is mainly evidenced in groups of directly related variables. Regarding the cardiovascular controller, it is evidenced that exclusion of the action of the central command (I-EP excluded) has a more significant impact than the exclusion of the central respiratory neuromuscular drive (NT excluded) on the sympathetic and parasympathetic efferent control activities, mainly intervening in HR and systemic arterial pressure measurements. Among the mechanisms that are related to the central command with the vascular resistances of the active muscles, the

exclusion of the vasodilator effect on peripheral resistance (I-R_{amp} excluded) stands out regarding the exclusion of the mechanism in venous resistance (V-R_{amv} Excluded), mainly affecting the cardiovascular variables. The exclusion of the muscle and respiratory pump mechanism (MP excluded and RP excluded, respectively) shows small effects in the model, which confirms that they are mechanisms of mild action, mainly related to systemic arterial pressures. Regarding respiratory variables, the most significant changes are related to the exclusion of the approach of minimization of mechanical work of breathing (minWOB excluded) and the effect of MRV on ventilation (MRV excluded), and due to the direct interaction with the gas exchange system, they also significantly affect the values of alveolar pressures. Finally, the exclusion of the use of blood flow signals in the gas exchange system (Q-GES excluded) shows a significant influence on alveolar gas partial pressures and systemic arterial pressures.

DISCUSSION

Cardiopulmonary Exercise Test Results

The general trend of the experimental data is consistent with what is expected for healthy adults under moderate exercise conditions, showing appropriate behaviors related to different mechanisms of the cardiorespiratory system regulation (see Fig. 2). The reached steady-state values for $\dot{V}CO_2$, $\dot{V}O_2$, HR, and $\dot{V}E$ at the end of the different phases and load steps of the cardiopulmonary exercise test are
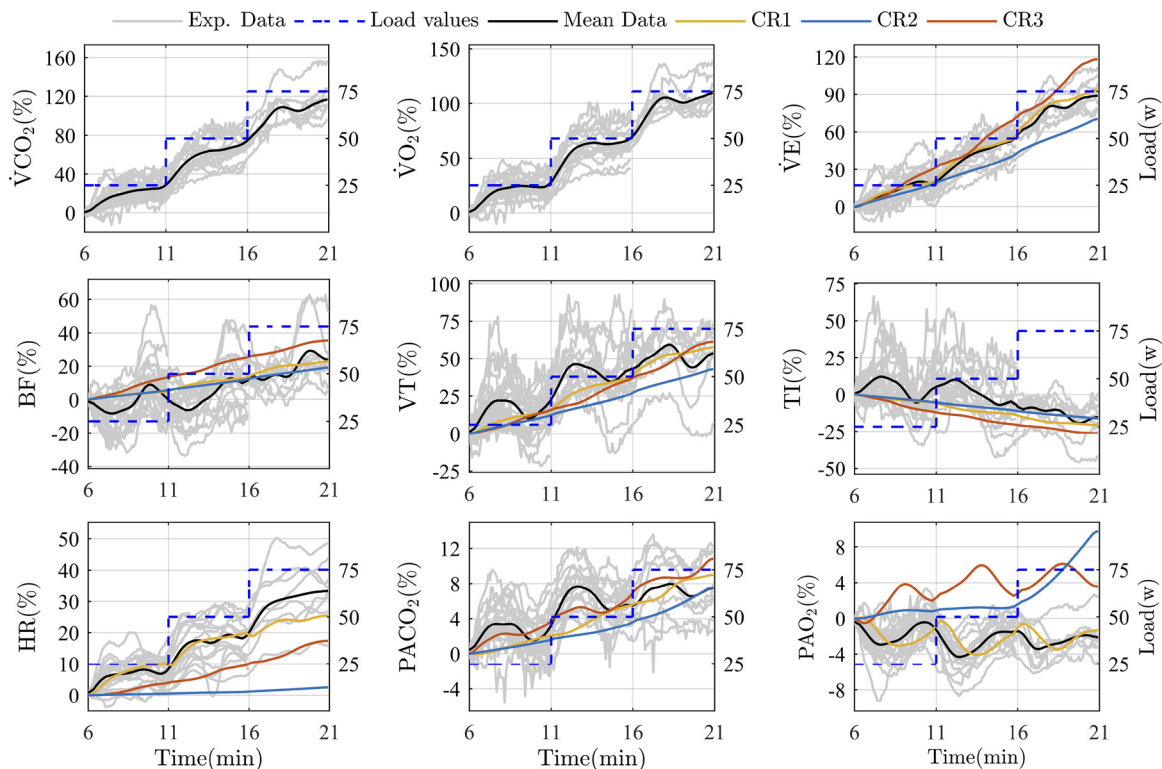

Figure 5. Transient simulation of continuous changes of the experimental values of $\dot{V}O_2$ and $\dot{V}CO_2$ in real time. For each variable as a function of time in minutes, solid yellow lines are the simulation results of CR1, solid blue lines are the simulation results of CR2, and solid orange lines are the simulation results of CR3. The results for each variable are compared with the experimental data corresponding to the simulated load steps, so that solid gray lines are the experimental data restricted by their respective anaerobic threshold (*AT*) and the solid black lines are their total mean value. The corresponding load values in watts of each step load simulated are shown as blue dashed lines.
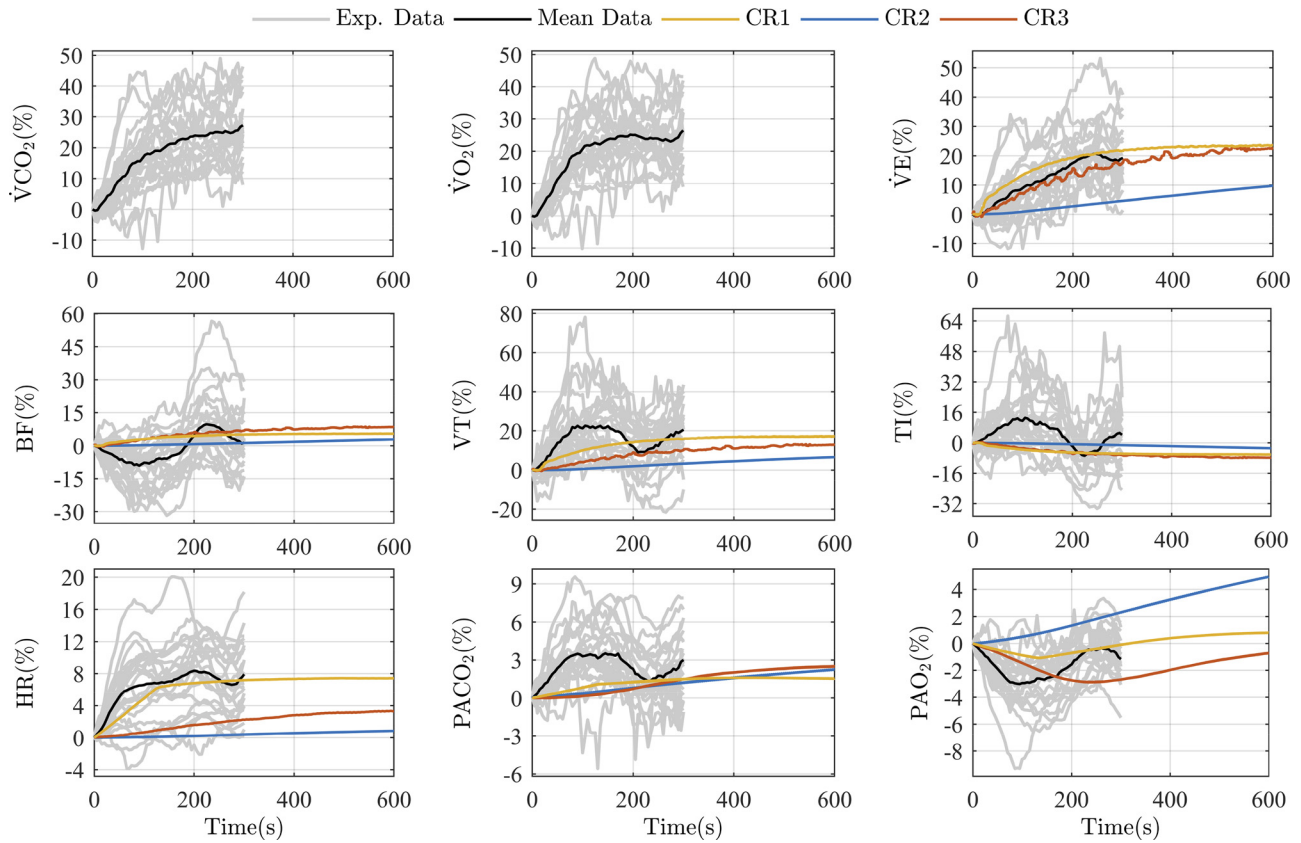
Figure 6. Transient simulation results to variations of $\dot{V}O_2$ and $\dot{V}CO_2$ as a single load step. The simulated step input corresponds to values from 0.64 to 0.82 L/min and from 0.58 to 0.76 L/min for $\dot{V}O_2$ and $\dot{V}CO_2$, respectively, that correspond to their mean values at the beginning and at the end of the first load step of the exercise phase in experimental data. For each variable as a function of time in seconds, solid yellow lines are the simulation results of CR1, solid blue lines the simulation results of CR2, and the solid orange lines the simulation results of CR3. The results for each variable are compared with the experimental data corresponding to the simulated load step so that solid gray lines are the experimental data restricted by their respective anaerobic threshold (*AT*) and solid black lines are their total mean value.

congruent with the selection criteria and designed protocol (8, 26, 28). The trend of the systemic blood pressure obtained under the increase in exercise load is congruent with the general description of the cardiovascular response for healthy subjects, characterized by a significant rise of PS, a slight rise in PM, and a slight decrease of PD (7, 28). The increase of $PACO_2$ and slight decrease of PAO_2 are typical metabolic responses under exercise and are related to the CO_2 production increase and the O_2 consumption increase by tissues (47, 48). General rises in BF and VT are also expected results (7), but the underdamped and contra-phase behavior of these variables, characterized by the initial

Table 13. *Settling time (in seconds) of the models for cardiorespiratory variables*

Model	$\dot{V}E$	VT	BF	TI	$PACO_2$	PAO_2	HR
CR1	280.8	277.9	290.4	277.9	2,544.6	2,831.0	290.6
CR2	2,555.7	2,476.5	2,594.7	2,563.6	2,356.5	2,424.2	2,429.3
CR3	729.8	753.3	711.5	711.5	1,309.6	2,809.8	1,203.4

The values correspond to the settling times in seconds of each models' predictions calculated only for the continuously recorded cardiorespiratory variables. BF, breathing frequency; HR, heart rate; $PACO_2$, alveolar partial pressure of CO_2; PAO_2, alveolar partial pressure of O_2; TI, inspiratory time; $\dot{V}E$, minute ventilation; VT, tidal volume.

decrease of BF and increase in VT after the load change, is an interesting finding because it evidences characteristics of the respiratory regulation mechanisms that are usually not described in the literature.

The magnitudes of some recorded variables like $\dot{V}E$, BF, $PACO_2$, and PAO_2 (see Fig. 2), mainly under rest conditions, differed from those found in similar experiments (5, 7). The resting condition defined in the implemented protocol (characterized by the registration of the subjects located in the cycle ergometer after a standing period during the instrumentation process), the anthropometric data recording, and the forced spirometry test explains the obtaining of some different resting values from those usually reported, mainly for respiratory variables $\dot{V}E$ and BF (5–8 L/min and 8–12 breaths/min, respectively) (5, 7). The resting values obtained for $PACO_2$ and PAO_2 are different from those usually reported (40 mmHg and 104 - 105 mmHg respectively) (5, 7, 48) due to differences in environmental conditions (mainly the atmospheric pressure) and the registered population characteristics, which is consistent with results of work related to acclimated subjects and under similar altitude conditions (49).

The sensitivity and linearity results regarding the workload allow for evaluating other characteristic aspects of cardiorespiratory regulation (see Table 8). The sensitivity
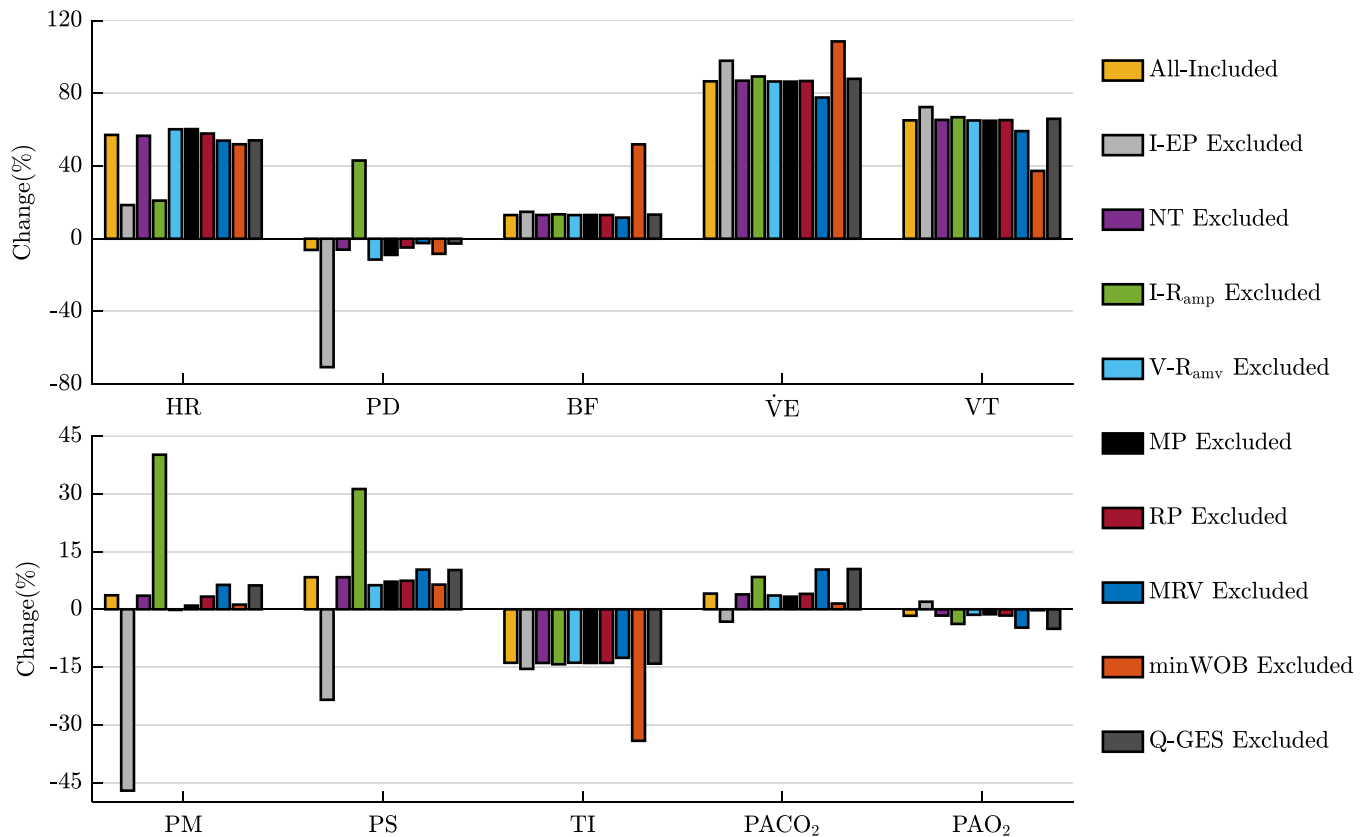
Figure 7. Steady-state %changes in CR1 predictions in response to an increase in stimulus from rest to an intermediate level of aerobic exercise, with all intact mechanisms and selective exclusions of each of them.

results of $\dot{V}CO_2$, $\dot{V}O_2$, $\dot{V}E$, VT, and HR in contrast with those obtained for PA_{CO_2} and PA_{O_2} show evidence of the response of cardiorespiratory regulation mechanisms to maintain O_2 and CO_2 blood concentrations near normal values during exercise. The high linearity and sensitivity of $\dot{V}CO_2$ and $\dot{V}O_2$ with respect to workload confirms their usefulness in both the assessment indices of the cardiorespiratory response in CPETs (28) and simulation inputs of models to relate the changes in exercise stimulus with metabolic changes. Differences among the linearity results also give an idea of undergoing regulation mechanisms of each variable concerning the workload. For example, less linear results obtained for PD, PA_{CO_2} and PA_{O_2} reflect more complex mechanisms of regulation than the more linear results obtained for $\dot{V}CO_2$, $\dot{V}O_2$, $\dot{V}E$, and HR.

Simulation

The regulatory mechanisms of CR2 and CR3 focus on maintaining the values of P_{sa}, $\dot{V}E$, VT, and arterial blood gas concentrations. However, the model parameter standardization and applied simulation inputs in this work lead to changes in the predictions regarding those reported [see the referenced works of Albanese et al. (20) and Serna et al. (21)]. Altitude increase regarding sea level, which is related to partial pressures decreasing inspired O_2 and CO_2, directly affects the gas exchange system of every model and implies lower values of PA_{CO_2} and PA_{O_2} (see Fig. 3). A decreasing of the parameter's values related to the blood volumes (see Table 11)

has a direct effect on the model systems and controllers. This fact leads to changes as lower systemic blood pressures (mainly PS and PD) and higher $\dot{V}E$ result in response to disturbances in blood gas concentrations (lower PA_{O_2} and higher PA_{CO_2}) caused by lower blood flow. This behavior can be evidenced mainly for CR2 (see Fig. 3). Changes in all of the predictions are related to the used $\dot{V}O_2$ and $\dot{V}CO_2$ values that, under rest conditions and incremental exercise, correspond to magnitudes that differ from what is usually reported (see Table 10). Considering that CR2 keeps the I:E ratio constant, its increase is directly related to a higher TI value and, therefore, also with morphological changes that imply higher magnitudes of the VT and $\dot{V}E$ signals. This is a weakness of CR2.

The results obtained showed that CR1 could reproduce the experimental data globally with greater fidelity compared with CR2 and CR3. Because of the three models establishing their parameter values considering basically the same subject (20, 21) and that the simulation conditions for all the models were standardized with respect to the experimental data, the resulting differences could be mainly related to the difference among the mechanisms implemented in each model. First, regarding the improvement of the simulation in the cardiovascular system and controller, the physiological mechanisms included in CR1 have been crucial: the inclusion of the central command and the central respiratory neuromuscular drive, the differentiation of the vascular beds into active and resting skeletal muscles, and the consideration of the muscle and respiratory pump regarding the

venous return. Second, about the respiratory system, the results of CR1 are related to the adjustment of the respiratory pattern implemented in the controller, based on the optimization approach of the minimal work of breathing. Finally, the main difference in the gas exchange system is related to the use of blood flow signals of the tissues and the brain directly from the cardiovascular system. The effect of these mechanisms regarding the results is discussed in detail below.

Steady-state response.
The experimental results for HR show an approximately linear increase in dynamics regarding $\dot{V}CO_2$ rise, as expected for the stimulus (8). The three models explain this behavior by a linear relationship between the sympathetic and parasympathetic responses regarding the same basal value (see *Eq. 119* in the Supplemental Material) (20, 21). In general, prediction differences among the models could be related to the cardiovascular controller inputs (see Fig. 1), the mechanisms involved with the sympathetic and parasympathetic response, and the associated parameter values. The predictions of CR2 and CR3 exhibit linear behaviors regarding $\dot{V}CO_2$, which are differentiated by their resting values and slopes (see Fig. 3). Considering the similarity between the controller components of CR2 and CR3, these differences can be attributed to the parameter values used in each case, corresponding to those indicated by each model authors [see the works by Albanese et al. (20) and Serna et al. (21)]. In contrast, CR1 shows a more complex response (nonlinear regarding the stimulus level), and consistent with experimental data. Such behavior is mainly associated with the addition of mechanisms related to the aerobic exercise dynamics (see Fig. 3 and *Cardiovascular controller*). With respect to prediction capability, CR1 and CR3 were the closest to the experimental data, without any significant statistical difference between them. At the same time, CR2 was the model with the worst prediction because the values of the implemented parameters are related to a sympathetic/parasympathetic activity ratio that was lower than expected (see Fig. 4). The response of CR1 at rest is less than expected due to the adoption of CR2 parameter values. Still, because of the addition of the central command effect, it exhibits a parabolic profile that adequately approaches the experimental data under stimulus level increases (see *Cardiovascular controller*).

The behavior of systemic blood pressures (PD, PM, and PS) is represented by the models hereon compared as an indirect result of sympathetic and parasympathetic activities on the cardiovascular system (see *Eq. 2* in the Supplemental Material) (20, 21). In this sense, the differences found among the models' predictions can be associated mainly with their cardiovascular regulation variables and the mechanisms applied in their cardiovascular systems. For instance, the cardiovascular parameters of CR2 are related to a low sympathetic/parasympathetic activity ratio compared with the other models, displaying blood pressure predictions with low resting values and a linear behavior with a slow positive slope when exercising increases (see Fig. 3). CR3 also exhibits a linear response with a positive slope for all blood pressures under stimulus increments, but its cardiovascular parameters, which are related to a higher sympathetic/parasympathetic activity ratio, leads to predictions with higher resting

values and slopes, getting a better prediction for PS (see Fig. 4). Like in HR, CR1 is the only model with a nonlinear response for blood pressure during aerobic exercise. This behavior can be associated with the exercise mechanisms implemented in the model and the respiratory controller that regulates the respiratory mechanics variables (see *Cardiovascular system* and *Cardiovascular controller*). Although CR1 does not present the best PE results for PS and PM, it is the only one with a similar dynamic for PD during exercise.

Regarding the respiratory mechanic variables ($\dot{V}E$, VT, BF, and TI), all of the models show predictions with similar dynamics to those expected but with significant differences regarding their precision. During exercise, increments of $\dot{V}E$, VT, and BF are expected as a result of increased metabolic demand (8). TI values trend to remain stable or slightly decrease, which is, in turn, associated with the change of BF and decrease of TE. CR2 respiratory controller is the simplest one. It is characterized by keeping the I:E ratio constant, regulating BF only as a function of Pa_{CO_2} and Pa_{O_2}. It does not include any exercise-related mechanism, so it presents the weak predictions. The most accurate results are obtained for CR1 and CR3, whose respiratory controllers consider the information of several chemoreceptors to set $\dot{V}E$ and involve mechanisms focused on the optimization of the respiratory pattern directly related to BF, TI, and VT. Considering the similarity between CR1 and CR3 systems and controllers and the role of their chemoreceptors for regulation, the best overall result obtained by CR1 can be attributed both to the optimization approach based on minimal work of breathing and to the changes implemented in the gas exchange system (see *Respiratory controller* and *Gas exchange system*).

Concerning the gas exchange subsystem variables, CR1 and CR3 were the models presenting dynamics and values closest to those observed experimentally (see Figs. 3 and 4 and Table 12). The behavior of these variables, characterized by a slight decrease of PA_{O_2} and an increase of PA_{CO_2}, reflects the interaction of cardiovascular and respiratory mechanisms to maintain the O_2 and CO_2 levels as a result of metabolic activity under exercise (8). Although all the compared models integrate mechanisms that involve increases in blood flow and ventilatory demand and consider changes in the concentrations of gases at venous and arterial levels in different tissues under exercise, the best results are related to the proper balance between these dynamics. In this sense, the atypical behavior of CR2 regarding PA_{O_2} reveals the restriction of this model to simulate exercise, mainly because it quickly reaches the saturation limit of O_2 concentration at the muscle level for $\dot{V}O_2$ values that exceed the resting state. Although CR1 and CR3 are based on the same gas exchange subsystem, the best results of CR1 can be related to an adequate balance between cardiovascular and respiratory functions related to the mechanisms involved in each system and controller and that the changes implemented regarding to brain and tissue perfusion represent in more detail the metabolism of gas concentrations (see Fig. 4 and *Gas exchange system*).

Transient response.
Considering that the transient responses under simulation of continuous stimulus changes can be understood as an

extension of the characteristics presented under the single load step simulation, the results of the second simulation setting are initially discussed (see Fig. 6 and Table 13).

The transient response of HR is represented with greater precision by CR1, which indicates that the implemented parameters and the mechanisms described by cardiovascular control, mainly due to their dynamic equations, are consistent with the behavior for this variable (see Fig. 6 and *Cardiovascular controller*). Same as for the steady-state response, the dynamic behavior of HR depends on the models' mechanisms regarding the regulation of the sympathetic/parasympathetic rate activity. The low sympathetic/parasympathetic rate activity associated with the CR2 parameters leads to predictions with a lower rate of change that do not stabilize during the simulation time (see Table 13). The effect of the exercise mechanisms implemented in CR1 differentiate it from CR3 and allows for obtaining the fastest prediction and highest rate of change, which coincides with experimental data.

The variables associated with respiratory mechanics in the transient regimen showed a great difference regarding to the models' predictions. (see Fig. 6). The behavior of $\dot{V}E$ concerning the increase in the stimulus for the models is related to general increases for both VT and BF (20, 21) (see Supplemental Material), and although this consideration is correct in steady state, in transitory response the underdamped and counterphase responses for both variables is not considered. The predictions of CR1 and CR3 show behaviors close to the experimental data of $\dot{V}E$, mainly because the ventilatory control of both models focuses directly on the prediction of this variable. The transient experimental data from BF, TI, and VT exhibit regulatory processes of greater complexity than the mechanisms implemented in all models despite the variability between the pulmonary mechanics and the respiratory pattern optimizers implemented in each one.

CR2 was characterized by presenting the slowest response, in which none of the predictions reaches the steady-state phase, and therefore, it is not possible to show any complete dynamic behavior despite the apparently good general result for BF and TI. (see Fig. 6 and Table 13). This result is obtained considering that, despite including a very detailed respiratory mechanics model, it implements the simplest respiratory controller, which in combination with the values assigned to parameters (mainly those related to gains and delays) generates the slowest predictions.

CR1 and CR3 implement similar respiratory mechanics that in combination with their own control mechanisms allow predictions that reach the settling of all variables and predict the experimental response more adequately (see Fig. 6 and Table 13). Although the CR1 controller is the most complex one, the settling times of its predictions are the shortest and closest to the experimental data due to its optimization regarding the evaluation of the ventilatory changes in the physiological range (see *Respiratory controller*). Even so, apart from $\dot{V}E$, the CR1 and CR3 simulations could not properly predict the dynamics of the experimental responses, an aspect that put in evidence the lack of a specialized subsystem for these models to reproduce the transient response under exercise.

The experimental results of PA_{CO_2} and PA_{O_2} also showed dynamics that could not be correctly predicted by the models, which shows evidence of the lack of specificity of all models regarding the mechanisms involved in the transitory regime for gas exchange (see Fig. 6). Soon after a change of exercise level, a decrease in PA_{O_2} and an increase in PA_{CO_2} are obtained due to the slow rise in $\dot{V}E$ compared with $\dot{V}O_2$ and $\dot{V}CO_2$ respectively (see Fig. 6); later, this behavior is reversed, PA_{O_2} reaches a stable value close to its resting state, and PA_{CO_2} reaches higher values than its resting state (depending on the subject's degree of apprehension, anxiety, and training) (6). The CR2 results are associated with the low rate of change and slowness of the cardiovascular and respiratory system responses, combined with its limitation to regulate oxygen concentrations when the stimulus increases (see Table 13). Although CR1 and CR3 are based on the same gas exchange system, the most accurate predictions of CR1 are related to the variation regarding the brain and tissue perfusions (see *Gas exchange system*) and an adequate balance of cardiovascular and ventilatory contribution, even with dynamics that are closer to the experimental. Even so, it is emphasized that the variables of this subsystem, both experimentally obtained and predicted by the models, are the ones that take the longest to reach the steady state. It is highlighted that the experimental values of PA_{CO_2} and PA_{O_2} are approximations (see *Eqs. 1* and *2)*, so the results could be different if the comparison is made with real measurements of these variables.

The results of continuous stimulus changes show evidence of different aspects of the models' characteristics, especially considering the shorter simulation times, the different levels of exercise, and the less abrupt variations of the stimulus. Regarding HR, the CR1 prediction was considerably different in the last stimulus level from the mean experimental result, which is justified considering that the calculated *AT* mean value (used as a central command mechanism parameter) was exceeded for that stimulus level (see Table 9). The best CR1 prediction for $\dot{V}E$ corroborates the good response of this model in terms of speed and rate of change, evidenced too in the single-step load simulation results. For BF, VT and TI, it was confirmed that none of the models are able to correctly predict their transient dynamics, although the best result was that obtained by CR1, and it is highlighted that the good results of CR2 are due to the coincidence of its slow response regarding the experimental data rate of change (see Figs. 5 and 6). For the gas exchange system, the CR1 rapid response and the adequate predictions are confirmed, especially for the PA_{O_2}, and the CR2 limitation about the O_2 regulation is evidenced again, albeit for higher stimulus values due to its slow response speed.

Sensitivity analysis.

The exclusion of the central command action on sympathetic and parasympathetic efferent control activities (I-EP excluded) has one of the most significant effects with respect to the entire model (see Fig. 7). The impact of this modification is evidenced mainly by the decreases in HR and the systematic blood pressure measurements, which are due to the absence of its action to increase sympathetic activity and reduce parasympathetic activity during exercise (see *Eqs. 108* and *111* in the Supplemental Material). Consequently, the level of cardiac output is affected and, therefore, the blood gas regulation, presenting variations in the behavior of

PA_{CO_2} and PA_{O_2}. The respiratory controller also modifies its behavior in relation to the blood gas exchange, presenting increases in $\dot{V}E$, BF, and VT and a decrease in TI.

Like the central command, the central respiratory neuromuscular drive (NT) has an action to increase sympathetic activity and decrease parasympathetic activity during exercise, but the results of excluding this mechanism (NT Excluded) show that its contribution is not so significant for the evaluated level of the stimulus. This behavior is related to active participation only during the inspiratory time interval (see *Eqs. 11* and *12*). In accordance with the above, this mechanism could be related to mild actions in the regulation of cardiovascular activity, which is mostly evident in the transitory regime of predictions.

The vasodilatory action on active muscles due to central command is also one of the mechanisms whose exclusion has a significant effect on the model (I-R_{amp} excluded). When blocking it, as expected during exercise, an increase in systemic arterial pressure measurements (PD, PM and PS) is evidenced because peripheral resistance is higher compared with that of the model that preserves all mechanisms. Due to the above, the cardiovascular controller decreases HR, but the cardiac output is also modified and, in turn, affects the gas exchange system. Although the respiratory controller decreases TI and increases $\dot{V}E$, VT, and BF, the higher value of PA_{CO_2} and lower value of PA_{O_2} occur during exercise.

Excluding the separate description of the venous vascular beds from active muscles (V-R_{amv} excluded) also affects the blood flows and systemic arterial pressure, but its effect is contrary to the vasodilatory action on active muscles due to central command (I-R_{amp}). As a result of this modification, lower systemic arterial pressure measurements are obtained, which involve slight modifications of the cardiovascular regulation and blood gas exchange and are related to an increase in PA_{O_2}, and a decrease in PA_{CO_2}. Considering that the variations in the gas exchange system for the evaluated stimulus level are not significant, there are no changes in the respiratory variables.

The action of the muscle pump is related to the increase in pressure in the venous vascular beds during exercise (see *Eqs. 4–6*), which is why its exclusion (MP excluded) is evidenced as a decrease in the baseline of systemic arterial pressure. This is evidenced as a decrease in the variation in PS, a very low variation in PM, and an increase in the negative variation in PD. Even so, these changes imply slight variations in the regulation of cardiovascular control and gas exchange system and nonsignificant changes in respiratory variables.

The respiratory pump is a mechanism that also affects venous blood return through pressure changes in the vascular beds (see *Eqs. 7* and *8)*, and its exclusion (RP excluded) is evidenced as a decrease in PS and an increase in PD. These results, unlike the muscular pump, are related to the fact that its action not only influences the systemic vascular compartments but also those related to the pulmonary and cardiac blood circulation (see Supplemental Material), affecting the amplitude of the systemic arterial pressure signal. Even so, the changes due to their exclusion are very slight for the level of stimulus evaluated, so no significant changes are observed in the behavior of other variables.

The exclusion of the neural driving component metabolically related to ventilation (MRV excluded) is directly associated with the decrease in $\dot{V}A$ and, therefore, is shown as a decrease in the variation of $\dot{V}E$ (see *Eqs. 135* and *138* in Supplemental Material). In accord with the approach of minimization of mechanical work of breathing, the equivalent respiratory pattern is associated with decreases in variation of BF, VT and TI. This significantly affects gas exchange and promotes slight changes in cardiovascular variables, but finally, higher values of PA_{CO_2} and lower values of PA_{O_2} are evidenced compared with the model that has all mechanisms intact.

The exclusion of respiratory pattern optimization approach and the change in the respiratory mechanics (minWOB excluded) involves modifications in the behavior and values of respiratory variables, like those obtained with CR3 due to the similarity of the controller and the system (see Fig. 3). In this sense, the changes shown in respiratory variables should be evaluated considering variations in their values even at rest. The increase in the change evidenced in $\dot{V}E$, TI, and BF and the decrease in VT are related to variations in PA_{CO_2} and PA_{O_2} lower than those of the model with all mechanisms intact. Although the results of the exclusion of these mechanisms could be associated with a more adequate regulation of gas exchange, the predictions of the respiratory variables are more distant with respect to the experimental data, contributing to a greater prediction error of the model. This is due mainly to obtaining lower values of $\dot{V}E$ and VT and higher values of TI both in exercise and at rest.

The results of excluding the use of blood flow signals from the cardiovascular system in the gas exchange system (Q-GES excluded) show that this modification is one of the most significant with respect to the regulation of PA_{O_2} and PA_{CO_2} during exercise. These changes show evidence of the difference between evaluating continuous variations of cardiovascular regulation in the gas exchange system and assigning a percentage of total cardiac output to the brain and tissue perfusion.

Application, Limitations, and Future Work

In this work, three cardiorespiratory models were compared under simulation of aerobic exercise in healthy adult humans. Standardization of all models was performed in order to compare them under simulation conditions as close as possible to the experimental data of reference. According to the obtained results, the proposed model can be considered the most appropriate one to predict the cardiorespiratory response of healthy human subjects under incremental exercise stimuli, environmental conditions, and characteristics of the studied data set. The benefits of the proposed model will depend on the specific simulation interests, that is, a proper cardiovascular response or respiratory mechanisms or only gas exchange variables. This can be evaluated from the resulting figures and prediction errors presented in the study. These best results can be attributed to the systems, controllers, and mechanisms integrated and adapted that allow for representing more adequately the behaviors, functions, and interactions of the different cardiorespiratory elements. In particular, the proposed model improves the ability of previous ones to predict the cardiorespiratory response to exercise, especially the transient and steady-state responses of $\dot{V}E$, HR, and blood arterial pressures (PS,

PM, and PD; see Figs. 3–6). Moreover, they are congruent with the criteria applied in the work of Cheng et al. (1), Summers et al. (50), and Hester et al. (51), which considers that a computational model of a physiological system is valid when its results are directionally appropriate and its steady-state predictions approximate experimental data and demonstrate responses that are reasonably accurate during dynamic transitions.

The purpose of the integrated model proposed in this work is to provide a useful system for clinical applications related to diagnosis, monitoring, education, and research. These applications are mainly justified by the ability to *1*) to represent different functions, dynamics, and interactions of the cardiorespiratory system, *2*) simulate different environmental conditions, disturbances, and subjects' characteristics modifying available parameters, and *3*) predict important cardiorespiratory variables recorded in cardiopulmonary exercise tests.

Future applications of the model could be related to the analysis of cardiorespiratory diseases during exercise tests, simulation of respiratory and cardiovascular therapeutic interventions, and development of personalized diagnostic tools. Although no pathology was considered in this work, due to the different characteristics and mechanisms included in the proposed model, it could be adequate to represent several environmental and pathological conditions after a fitting and validation with specific population data. Moreover, the model could be used to predict the effect of therapeutic interventions by its simulation with changes in related parameters (i.e., the cardiorespiratory response of a respiratory patient undergoing mechanical ventilation). Similar to cardiorespiratory diseases, the model could be fitted for specific conditions and characteristics of a subject, getting personalized predictions useful for predictive and preventive medical applications.

According to the characteristics and previous evaluations of the models on which this study was based, the ability of the proposed model to simulate the cardiorespiratory response of healthy human subjects under stimuli of hypercapnia and hypoxia can also be considered (22, 23, 40). The evaluation of the ability to simulate these stimuli would be similar work to that presented in this paper, comparing the predictions of the proposed model with experimental data and simulation results of other models under the specific disturbances.

It is highlighted that each integrated and studied model included in this work was designed to be simulated under specific environmental conditions, subjects' characteristics, and stimuli. Even so, despite the differences between these specifications and constraints regarding the characteristics of the experimental procedure, the simulation of each model was compared to determine which one would be the most suitable model to predict the response of a subject under a cardiopulmonary exercise test, like experimental data registered in this study, from a model structure perspective.

Among the main restrictions that determine the usefulness of the proposed model are as follows. It is possible only to perform simulations in which the posture of the subject remains constant because the effects of gravity were not included, the model is only suitable for simulation of exercise below *AT* because mechanisms related to anaerobic

activity were not considered, and the model is suitable only for short-term regulation because it does not include hormonal or related mechanisms.

Considering the structural approach of the evaluation applied in this work, and despite the good results obtained, a detailed parameter's fitting of the proposed model should be applied in order to improve its prediction capacity and completely validate it, even under different stimuli. This methodology could comprise a sensitivity analysis of parameters involving optimization techniques that allow for minimizing the differences between model predictions and experimental data. It allows for identifying the most sensitivity parameters and tuning them (into a physiologically bounded searching space) to fit the model to experimental data. After that, parameter adjustment to a specific subject could be considered to aim to get a personalized model and, in this way, move toward the development of a personalized diagnostic and forecast system.

It is important to note that the parameter values' validation will depend on the overall parameter fitting to either population or subjects' characteristics, environmental conditions, and stimulus type. The hereon proposed model involves a large parameter number, whereas experimental measurement quantity is restricted. Therefore, it is possible to find different sets of parameter values that lead to the same result during the fitting procedure for conditions like hereon addressed (13). For this reason, it is necessary to consider complexity of reduction techniques, subset selection, and sensitivity analysis that allows for identifying only the limited number of parameters that need to be fitted to predict experimental data correctly.

Conclusions

This paper presents a new integrated mathematical model focused on simulating the cardiorespiratory response of a healthy human under resting and aerobic dynamic exercise conditions. This evolved model adapts different mechanisms and components for the cardiovascular system, respiratory mechanics, gas exchange system, and the respiratory and cardiovascular controllers, which makes it suitable for the prediction of different physiological variables both in steady-state and in transient responses.

DISCLOSURES

No conflicts of interest, financial or otherwise, are declared by the authors.

AUTHOR CONTRIBUTIONS

C.A.S. and A.M.H. conceived and designed research; C.A.S. performed experiments; C.A.S. and L.Y.S. analyzed data; C.A.S., A.M.H., L.Y.S., M.A.M. interpreted results of experiments; C.A.S. prepared figures; C.A.S. and L.Y.S. drafted manuscript; C.A.S., A.M.H., L.Y.S., M.A.M. edited and revised manuscript; C.A.S., A.M.H., L.Y.S., M.A.M. approved final version of manuscript.

REFERENCES

1. **Cheng L**, **Albanese A**, **Ursino M**, **Chbat NW.** An integrated mathematical model of the human cardiopulmonary system: model validation under hypercapnia and hypoxia. *Am J Physiol Heart Circ Physiol*

310: H922–H937, 2016. doi:https://doi.org/10.1152/ajpheart.00923.2014.

2. **Poon CS.** Ventilatory control in hypercapnia and exercise: optimization hypothesis. *J Appl Physiol (1985)* 62: 2447–2459, 1987. doi:https://doi.org/10.1152/jappl.1987.62.6.2447.

3. **Cardona-Morrell M**, **Prgomet M**, **Turner RM**, **Nicholson M**, **Hillman K.** Effectiveness of continuous or intermittent vital signs monitoring in preventing adverse events on general wards: a systematic review and meta-analysis. *Int J Clin Pract* 70: 806–824, 2016. doi:https://doi.org/10.1111/ijcp.12846.

4. **Silva SCd**, **Monteiro WD**, **Farninatti PdTV.** Exercise maximum capacity assessment: a review on the traditional protocols and the evolution to individualized models. *Rev Bras Med do Esporte* 17: 363–369, 2011. doi:https://doi.org/10.1590/S1517-86922011000500014.

5. **Guyton A**, **Hall J.** *Textbook of Medical Physiology*, 11th ed. Philadelphia, PA: Saunders, 2006.

6. **Wasserman K**, **Hansen J**, **Sietsema K**, **Sue DY**, **Stringer WW**, **Sun XG**, **Whipp BJ.** *Principles of Exercise Testing and Interpretation: Including Pathophysiology and Clinical Applications*, 5th ed. Philadelphia, PA: Lippincott Williams & Wilkins, 2012.

7. **Cooper CB**, **Storer TW.** *Exercise Testing and Interpretation*, 1st ed. Cambridge, UK Cambridge University Press, 2001.

8. **Heyward V**, **Gibson A.** *Advance Fitness Assessment and Exercise Prescription*, 7th ed. Champaign, IL: Human Kinetics, 2014.

9. **Batzel JJ**, **Kappel F**, **Schneditz D**, **Tran HT.** *Cardiovascular and Respiratory Systems: Modeling, Analysis, and Control*, 1st ed. Philadelphia, PA: SIAM, 2007.

10. **Marmarelis VZ.** *Nonlinear Dynamic Modeling of Physiological Systems*. 1st ed. Hoboken, NJ: John Wiley & Sons, Inc., 2004.

11. **Batzel JJ**, **Bachar M**, **Karemaker JM**, **Kappel F.** *Mathematical Modeling and Validation in Physiology*. Berlin Heidelberg, Germany: Springer, 2013.

12. **Lu K**, **Clark JW Jr**, **Ghorbel FH**, **Ware DL**, **Bidani A.** A human cardiopulmonary system model applied to the analysis of the Valsalva maneuver. *Am J Physiol Heart Circ Physiol* 281: H2661–H2679, 2001. doi:https://doi.org/10.1152/ajpheart.2001.281.6.H2661.

13. **Ellwein LM**, **Pope SR**, **Xie A**, **Batzel JJ**, **Kelley CT**, **Olufsen MS.** Patient-specific modeling of cardiovascular and respiratory dynamics during hypercapnia. *Math Biosci* 241: 56–74, 2013. doi:https://doi.org/10.1016/j.mbs.2012.09.003.

14. **Poon CS**, **Lin SL**, **Knudson OB.** Optimization character of inspiratory neural drive. *J Appl Physiol (1985)* 72: 2005–2017, 1992. doi:https://doi.org/10.1152/jappl.1992.72.5.2005.

15. **Fincham WF**, **Tehrani FT.** A mathematical model of the human respiratory system. *J Biomed Eng* 5: 125–133, 1983. doi:https://doi.org/10.1016/0141-5425(83)90030-4.

16. **Magosso E**, **Ursino M.** Cardiovascular response to dynamic aerobic exercise: a mathematical model. *Med Biol Eng Comput* 40: 660–674, 2002. doi:https://doi.org/10.1007/BF02345305.

17. **Cheng L**, **Khoo MC.** Modeling the autonomic and metabolic effects of obstructive sleep apnea: a simulation study. *Front Physiol* 2: 111, 2011.

18. **Hernández AM.** *Sistema de control respiratorio ante estímulos y patologías: Análisis, Modelado y Simulación*. OmniScript. Publicia, 2014.

19. **Mananas MA**, **Hernandez AM**, **Romero S**, **Grino R**, **Rabinovich R**, **Benito S**, **Caminal P.** Analysis of respiratory models at different levels of exercise, hypercapnia and hypoxia. In: *Proceedings of the 25th Annual International Conference of the IEEE Engineering in Medicine and Biology Society (IEEE Cat. No.03CH37439)*. IEEE, p. 2754–2757.

20. **Albanese A**, **Cheng L**, **Ursino M**, **Chbat NW.** An integrated mathematical model of the human cardiopulmonary system: model development. *Am J Physiol Heart Circ Physiol* 310: H899–H921, 2016. doi:https://doi.org/10.1152/ajpheart.00230.2014.

21. **Serna LY**, **Mañanas MA**, **Hernández AM**, **Rabinovich RA.** An improved dynamic model for the respiratory response to exercise. *Front Physiol* 9: 69, 2018. doi:https://doi.org/10.3389/fphys.2018.00069. .

22. **Cheng L**, **Ivanova O**, **Fan HH**, **Khoo MC.** An integrative model of respiratory and cardiovascular control in sleep-disordered breathing. *Respir Physiol Neurobiol* 174: 4–28, 2010. doi:https://doi.org/10.1016/j.resp.2010.06.001.

23. **Magosso E**, **Ursino M.** A mathematical model of CO2 effect on cardiovascular regulation. *Am J Physiol Heart Circ Physiol* 281: H2036–H2052, 2001. doi:https://doi.org/10.1152/ajpheart.2001.281.5.H2036.

24. **Ursino M**, **Magosso E.** Acute cardiovascular response to isocapnic hypoxia. I. A mathematical model. *Am J Physiol Heart Circ Physiol* 279: H149–H165, 2000. doi:https://doi.org/10.1152/ajpheart.2000.279.1.H149.

25. **Gibbons JD**, **Chakraborti S.** *Nonparametric Statistical Inference*. 4th ed. New York: CRC Press, 2011.

26. **Latin RW**, **Berg KE**, **Smith P**, **Tolle R**, **Woodby-Brown S.** Validation of a cycle ergometry equation for predicting steady-rate VO2. *Med Sci Sports Exerc* 25: 970–974, 1993.

27. **Evans CH**, **White RD.** *Exercise Stress Testing for Primary Care and Sports Medicine*. New York: Springer, 2009.

28. **American Thoracic Society, American College of Chest Physicians.** ATS/ACCP Statement on cardiopulmonary exercise testing. *Am J Respir Crit Care Med* 167: 211–277, 2003. doi:https://doi.org/10.1164/rccm.167.2.211.

29. **American College of Sports Medicine.** *ACSM's Guidelines for Exercise Testing and Prescription*. 9th ed. Philadelphia, PA: Lippincott Williams & Wilkins, 2013.

30. **Watanabe N**, **Reece J**, **Polus BI.** Effects of body position on autonomic regulation of cardiovascular function in young, healthy adults. *Chiropr Osteopat* 15: 19, 2007. doi:https://doi.org/10.1186/1746-1340-15-19.

31. **Van Iterson EH**, **Olson TP.** Use of "ideal" alveolar air equations and corrected end-tidal PCO2 to estimate arterial PCO2 and physiological dead space during exercise in patients with heart failure. *Int J Cardiol* 250: 176–182, 2018. doi:https://doi.org/10.1016/j.ijcard.2017.10.021.

32. **Jones NL**, **Robertson DG**, **Kane JW.** Difference between end-tidal and arterial PCO2 in exercise. *J Appl Physiol Respir Environ Exerc Physiol* 47: 954–960, 1979. doi:https://doi.org/10.1152/jappl.1979.47.5.954.

33. **Thomas V**, **Costes F**, **Busso T.** Estimation of arterial PCO2 from a lung model during ramp exercise in healthy young subjects. *Respir Physiol Neurobiol* 156: 259–265, 2007. doi:https://doi.org/10.1016/j.resp.2006.11.004.

34. **Bengtsson J**, **Bake B**, **Johansson A**, **Bengtson JP.** End-tidal to arterial oxygen tension difference as an oxygenation index. *Acta Anaesthesiol Scand* 45: 357–363, 2001. doi:https://doi.org/10.1034/j.1399-6576.2001.045003357.x.

35. **Mellemgaard K.** The alveolar-arterial oxygen difference: its size and components in normal man. *Acta Physiol Scand* 67: 10–20, 1966. doi:https://doi.org/10.1111/j.1748-1716.1966.tb03281.x.

36. **Riddle W**, **Younes M.** A model for the relation between respiratory neural and mechanical outputs. II. Methods. *J Appl Physiol Respir Environ Exerc Physiol* 51: 979–989, 1981. doi:https://doi.org/10.1152/jappl.1981.51.4.979.

37. **Younes M**, **Riddle W.** A model for the relation between respiratory neural and mechanical outputs. I. Theory. *J Appl Physiol Respir Environ Exerc Physiol* 51: 963–978, 1981. doi:https://doi.org/10.1152/jappl.1981.51.4.963.

38. **Younes M**, **Riddle W**, **Polacheck J.** A model for the relation between respiratory neural and mechanical outputs. III. Validation. *J Appl Physiol Respir Environ Exerc Physiol* 51: 990–1001, 1981. doi:https://doi.org/10.1152/jappl.1981.51.4.990.

39. **Otis AB**, **Fenn WO**, **Rahn H.** Mechanics of Breathing in Man. *J Appl Physiol* 2: 592–607, 1950. doi:https://doi.org/10.1152/jappl.1950.2.11.592.

40. **Serna Higuita LY**, **Mananas MA**, **Mauricio Hernandez A**, **Marina Sanchez J**, **Benito S.** Novel modeling of work of breathing for its optimization during increased respiratory efforts. *IEEE Syst J* 10: 1003–1013, 2016. doi:https://doi.org/10.1109/JSYST.2014.2323114.

41. **Hämäläinen RP**, **Sipilä A.** Optimal control of inspiratory airflow in breathing. *Optim Control Appl Meth* 5: 177–191, 1984. doi:https://doi.org/10.1002/oca.4660050209.

42. **Karamolegkos N**, **Albanese A**, **Isaza F**, **Chbat NW.** Patient emulator: A tool for testing mechanical ventilation therapies. In: *2016 38th Annual International Conference of the IEEE Engineering in Medicine and Biology Society (EMBC)*. IEEE, p. 4321–4324. doi:https://doi.org/10.1109/EMBC.2016.7591683.

43. **Vicario F**, **Albanese A**, **Wang D**, **Karamolegkos N**, **Chbat NW.** Constrained optimization for noninvasive estimation of work of breathing. In: *2015 37th Annual International Conference of the IEEE Engineering in Medicine and Biology Society (EMBC)*. IEEE, p. 5327–5330. doi:https://doi.org/10.1109/EMBC.2015.7319594.

44. **Ursino M**, **Magosso E.** A theoretical analysis of the carotid body chemoreceptor response to O2 and CO2 pressure changes. *Respir Physiol Neurobiol* 130: 99–110, 2002. doi:https://doi.org/10.1016/S0034-5687(01)00335-8.

45. **Harada T**, **Kubo H**, **Mori T**, **Sato T.** Pulmonary and Cardiovascular Integrated Model Controlled with Oxygen Consumption. *In: 2005 IEEE Engineering in Medicine and Biology 27th Annual Conference*. IEEE, p. 304–307. doi:https://doi.org/10.1109/IEMBS.2005.1616405.

46. **Magosso E**, **Cavalcanti S**, **Ursino M.** Theoretical analysis of rest and exercise hemodynamics in patients with total cavopulmonary connection. *Am J Physiol Heart Circ Physiol* 282: H1018–34, 2002. doi:https://doi.org/10.1152/ajpheart.00231.2001.

47. **Wasserman K**, **Whipp BJ.** Excercise physiology in health and disease. *Am Rev Respir Dis* 112: 219–249, 1975. doi:https://doi.org/10.1164/arrd.1975.112.2.219.

48. **Whipp BJ**, **Wasserman K.** Alveolar-arterial gas tension differences during graded exercise. *J Appl Physiol* 27: 361–365, 1969. doi:https://doi.org/10.1152/jappl.1969.27.3.361.

49. **Crapo RO**, **Jensen RL**, **Hegewald M**, **Tashkin DP.** Arterial blood gas reference values for sea level and an altitude of 1,400 meters. *Am J Respir Crit Care Med* 160: 1525–1531, 1999. doi:https://doi.org/10.1164/ajrccm.160.5.9806006.

50. **Summers RL**, **Ward KR**, **Witten T**, **Convertino VA**, **Ryan KL**, **Coleman TG**, **Hester RL.** Validation of a computational platform for the analysis of the physiologic mechanisms of a human experimental model of hemorrhage. *Resuscitation* 80: 1405–1410, 2009. doi:https://doi.org/10.1016/j.resuscitation.2009.09.001.

51. **Hester RL**, **Brown AJ**, **Husband L**, **Iliescu R**, **Pruett D**, **Summers R**, **Coleman TG.** HumMod: a modeling environment for the simulation of integrative human physiology. *Front Physiol* 2: 1–12, 2011.

52. **Baker RJ**, **Kozoll DD**, **Meyer KA.** The use of surface area as a basis for establishing normal blood volume. *Surg Gynecol Obstet* 104: 183–189, 1957.

53. **Mosteller RD.** Simplified calculation of body-surface area. *N Engl J Med* 317: 1098, 1987. doi:https://doi.org/10.1056/NEJM198710223171717.